Computational assessment of the fluorescence emission of phenol oligomers: A possible insight into the

(Article begins on next page)

18 September 2024

Computational assessment of the fluorescence emission of phenol oligomers: A possible insight into the fluorescence properties of humic-like substances (HULIS).

Francesco Barsotti,[a] Giovanni Ghigo,[b], Davide Vione [a],*

Dipartimento di Chimica, Università di Torino Via Giuria 5[a] and/or 7[b], 10125 Torino, Italy.

* Address correspondence to either author: *giovanni.ghigo@unito.it* (G. Ghigo, Phone +39-011-6707872), *davide.vione@unito.it* (D. Vione, Phone +39-011-6705296)

Abstract

Compounds with fluorescence in the humic-like substances (HULIS) region are known to be formed under conditions where the oxidation (which could lead to the oligomerization) of phenolic compounds is operational, because of the formation of phenoxy radicals. However, there was no evidence to date that such fluorescence emission was really due to phenol oligomers. In this work, the fluorescence of phenol and some of its oligomers was studied by computational methods and it was compared with experimental data, when allowed by the availability of commercial standards. The oligomer fluorescence depends on the contribution of different stable conformers, which differ from one another for the dihedral angles between the aromatic rings. Differences in the dihedral angles are also observed between the ground states and the corresponding excited singlet states. The predicted wavelengths of fluorescence emission increase with increasing the number of aromatic rings, up to a plateau at around 450 nm. Compounds with more than three-four aromatic rings are not expected to show emission in a different range, because the transitions causing fluorescence involve only three consecutive rings. These results support the hypothesis that oligomers account for the fluorescence emission in the HULIS region, which has been observed under the photochemical and photosensitized transformation of phenolic compounds.

Keywords: atmospheric photochemistry; oligomeric compounds; excitation-emission fluorescence matrix; phototransformation; density functional theory.

1. Introduction

Humic-like substances (HULIS) are important components of the atmospheric aerosols, of which they affect for instance the ability to nucleate water droplets and to absorb sunlight [1-3]. HULIS share some common features with humic and fulvic acids found in surface waters and soils (such as for instance the optical properties), but they are much smaller than humic acids and possess a smaller fraction of aromatic moieties and a larger fraction of aliphatic ones [4]. HULIS account for an important part of the water-soluble organic carbon in atmospheric aerosols, and they are thought to originate from both primary (biomass burning, release of organic compounds from water and soil to the atmosphere) and secondary processes (atmospheric reactions) [5-12].

The characterization of HULIS has been carried out with different techniques, including mass spectrometry, IR and NMR spectroscopy [13-16]. Unfortunately, these techniques often require sample fractionation and enrichment steps that would be problematic for a routine analysis of atmospheric samples. In contrast, characterization by absorption and fluorescence spectroscopy allows information to be obtained with minimal sample pre-treatment [17,18].

Several potential processes that could generate HULIS have been studied in the laboratory. Among these, photochemical reactions involving phenolic compounds in the presence of triplet sensitizers produce species with many similarities (functional groups, absorption and fluorescence spectra, hygroscopic properties) to atmospheric HULIS [19-23]. Interestingly, the same processes induce phenol oligomerization through the corresponding phenoxy radicals [19, 23-25]. Phenol oligomers might or might not account for the observed properties, because additional compounds would also be formed under the same conditions. However, phenols and HULIS emit in clearly separated wavelength intervals [17,26,27], and the photochemical and photosensitized transformation of phenols produces a gradual shift of the fluorescence emission range towards the HULIS region [23].

The testing of the hypothesis that the fluorescence in the HULIS region is accounted for by phenol oligomers (trimers, tetramers and so on) has to face the difficulty that these compounds are hardly available as commercial standards. To by-pass this problem, the present work carries out a quantum mechanical assessment of the fluorescence emission of phenol and of some of its oligomers, optimizing and validating the computational techniques by comparison with the available experimental data. By so doing, one can predict the fluorescence behavior of compounds for which standards are not available, and carry out a comparison with the known HULIS emission.

2. Materials and methods

The absorption spectra were measured with a Varian Cary 100 Scan UV-Vis double-beam spectrophotometer, using quartz cuvettes (1.000 cm optical path length). The excitation-emission

matrix (EEM) fluorescence spectra were taken with a VARIAN Cary Eclipse Fluorescence Spectrophotometer, with an excitation range from 200 to 400 nm at 10 nm steps, and an emission range from 200 to 600 nm with a scan rate of 1200 nm min^{-1}. Excitation and emission slits were set at 5 nm for 0.1 mM phenol (Aldrich, 99% purity grade) and at 20 nm for 0.1 mM 4-phenoxyphenol (Aldrich, 99%). Spectra were taken in a fluorescence quartz cuvette (Hellma) with 1.000 cm optical path length. The Raman signal of water was taken as a reference for lamp intensity and signal stability within different measurements.

The computational study was performed within the Density Functional Theory (DFT) [28-30] with the following procedure: we first optimized the geometries of the ground states, then we calculated the excitation energies with the Time- Dependent DFT (TD-DFT) [31,32]. This method provides a reasonable accuracy at reasonable computational costs (time and computing resources) [33-35]. The excitation energies calculated in this way correspond to the maxima in the absorption spectra, as this approach does not include vibrational contributions or dynamic solvent effects. Actually, our intent is not to fully reproduce the experimental absorption spectra, but only to identify the most important transitions and reproduce the fluorescence spectra. When more conformations are possible for a certain molecule, each set of transitions is reported scaled by the weight of the corresponding conformation (see details in the Supplementary Material, hereafter SM). In the following, each molecule was re-optimized in its first excited state, and the difference between its energy and the one calculated for the ground state at the excited state geometry was taken as emission (fluorescence) energy. Solvent effects (water) to the electronic energies were introduced both in geometry optimization and TD-DFT calculations by the Polarized Continuum Method (PCM) [36,37] within the universal Solvation Model Density [38,39]. There exist a wide variety of DFT functionals used in conjunction with the Time-Dependent approach. Therefore, a preliminary screening work was carried out and 17 different functionals were tested (see details in the SM). After the screening, we decided to use the mPWLYP functional (modified Perdew-Wang exchange functional) [40] and Lee-Yang-Parr correlation [41,42] with the Pople basis set 6-31+G(d) [43,44], because this method gives a suitable approximation of the experimental values and requests reasonable calculation time. Calculations were performed by the quantum package Gaussian 09-A [45]. Figures 2, 7 and SM1-SM7 (SM) and the Figures embedded in Tables in the SM were obtained with the graphical program Molden [46]. Figures 7 and SM2, SM4, SM6, SM7 in the SM show the differential electronic density maps at the excited state geometries in the electronic excitation, *i.e.* the graphic representation of the difference in electronic densities between the ground and the first excited state responsible for the fluorescence. In other terms, the red areas are where the electron comes from, while the blue area is where the electron goes (these areas roughly correspond to HOMO and LUMO in HOMO-LUMO dominated electronic transitions, as it is the case here).

3. Results and Discussion

The absorption and fluorescence properties were calculated for a series of poly-*para*-phenoxyphenols (Scheme 1): phenol, 4-phenoxyphenol (4PP), 4-(4-phenoxy)phenoxyphenol (4PPP) and 4-(4-(4-phenoxy)phenoxy)phenoxyphenol (4PPPP). For phenol and 4PP, the predictions of calculations were compared with the available experimental data. To confirm the predicted trend of the fluorescence emission wavelengths, partial calculations were also carried out for a 5-ring system (the latter calculations were referred to one conformation only, due to remarkable computational costs).
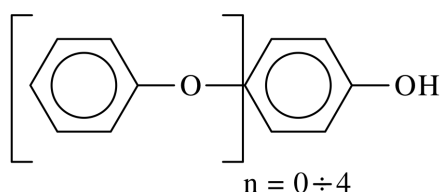

Scheme 1. **The poly-*para*-phenoxyphenols studied.**

3.1. Phenol

The absorption spectra were calculated as a first issue. Phenol absorption bands were predicted at <230 nm and at ~265 nm, in satisfactory agreement with the experimental data (see Figure 1a). As far as fluorescence is concerned, both the $S_2 \rightarrow S_0$ and $S_1 \rightarrow S_0$ transitions were calculated. For phenol, the predicted emission wavelengths (λ_{em}) were at 276 and 287 nm, respectively. Figure 1b reports the EEM spectrum of phenol, which shows fluorescence bands around excitation/emission (Ex/Em) wavelengths of ~220/~300 nm and ~270/~300 nm. The two bands with Ex/Em of ~220/~600 nm and ~270/~600 nm are the second harmonics of the bands with emission at ~300 nm.

The excitation wavelengths correspond quite well to the experimental and calculated absorption bands of phenol, while there appears to be only one emission band ($\lambda_{em} \sim 280\text{-}320$ nm). This band is consistent with the $S_1 \rightarrow S_0$ transition, in agreement with Kasha's rule [47] according to which the S_2 state would quickly undergo radiationless deactivation to S_1, from where the fluorescence emission would take place. The spectroscopic properties of phenol have been the subject of several computational studies, the more recent of which have been performed with high-level *ab-initio* methods [48-51]. However, these are not directly comparable with our results because all calculations have been carried out in the gas phase. More interesting is a comparison with experimental data [52,53] concerning the change in the structural parameters that is quite well reproduced (see details in SM).
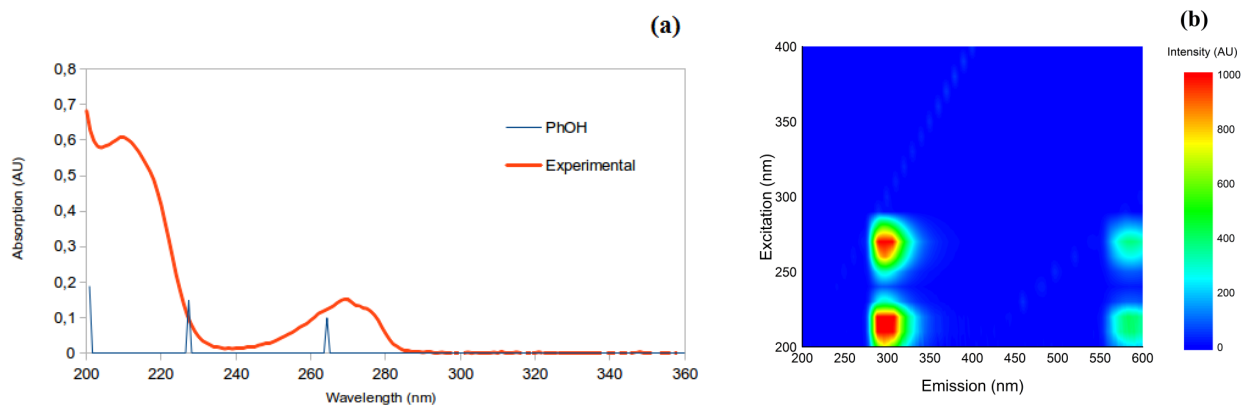
Figure 1. (a) **Experimental absorption spectrum of 0.1 mM phenol and calculated transitions (AU = absorbance units). (b) EEM matrix of 0.1 mM phenol in aqueous solution.**

3.2. 4-Phenoxyphenol

Differently from phenol that has just one conformer, 4-phenoxyphenol (4PP) has three different stable conformations (here indicated as 2a, 2b, 2c, see Figure 2). The main differences among the three conformers of 4PP are the two dihedral angles between the aromatic rings that, therefore, show different orientation one with respect to the other.

2a   **2b**   **2c**
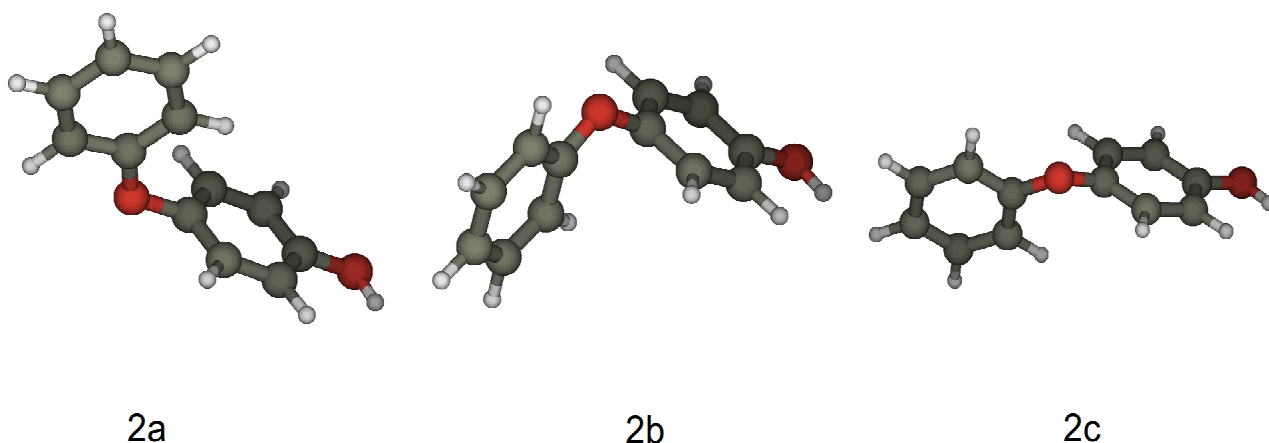
Figure 2. **The three conformers of 4-phenoxyphenol (4PP).**

Depending on the stability of each conformer, the relative abundance is predicted to be 2b > 2a > 2c. Eighty transitions were calculated for each structure, and they were superposed to the experimental absorption spectrum. Figure 3a shows the results of this procedure. The comparison suggests that the experimental absorption band of 4PP around 200 nm would be the result of

multiple transitions involving the three conformers. The experimental band around 230 nm would be produced by several transitions in the interval 220-240 nm, while the band around 280 nm would be the consequence of transitions taking place at 260-270 and 290-300 nm. Overall, there is a good qualitative agreement between the calculated transitions and the experimental spectrum.

To investigate the fluorescence properties of 4PP, the geometry of the first excited state of each conformer was determined. Based on the results obtained with phenol and in agreement with Kasha's rule, only the $S_1 \rightarrow S_0$ transition was taken into account. As for the ground state, the S_1 state presents, apparently, three conformations ($2aS_1$, $2bS_1$, $2cS_1$: their structures are reported in the SM) which differ, again, mainly for the values of the dihedral angles. Predicted transitions for the emission are at ~355 nm ($2a_{S_1 \rightarrow S_0}$) and ~425 nm (both $2b_{S_1 \rightarrow S_0}$ and $2c_{S_1 \rightarrow S_0}$). The former is due to an electron transfer from the π framework of the phenoxy moiety to the π framework of the phenol, while the latter are both due to an electron transfer in the opposite direction (Figure SM2).

The experimental fluorescence spectrum (EEM matrix) is reported in Figure 3b. It shows some linear features that do not depend on 4PP emission (they are the Raleigh scattering of the solution at $\lambda_{Em} = \lambda_{Ex}$, its second harmonic at $\lambda_{Em} = 2 \lambda_{Ex}$, and the Raman signal of water at $\lambda_{Em} > \lambda_{Ex}$), two weak fluorescence bands at Ex/Em wavelengths of ~220/~350 nm and ~280/~350 nm, and two more intense bands at Ex/Em ~220/~425 nm and ~300/~425 nm. The excitation wavelengths roughly correspond to the two absorption bands of 4PP at ~225 and ~280 nm ($S_0 \rightarrow S_2$ and $S_0 \rightarrow S_1$, respectively). Even more significantly, one observes a remarkably good agreement between the predicted and the observed wavelengths of fluorescence emission: a couple of weak bands correspond to the $2a_{S_1 \rightarrow S_0}$ transition, and the other couple to $2b_{S_1 \rightarrow S_0}$ and $2c_{S_1 \rightarrow S_0}$. The excited electronic states $2bS_1$ and $2cS_1$ are generated, respectively, from the 2b and 2c conformers which represent 70% of the population, while the electronic state $2aS_1$ is generated from 2a which is the remaining 30%. This can explain why the emission bands at ~350 nm (generated by $2aS_1$) are weaker than those found at ~425 nm (generated by the most abundant $2bS_1$ and $2cS_1$).
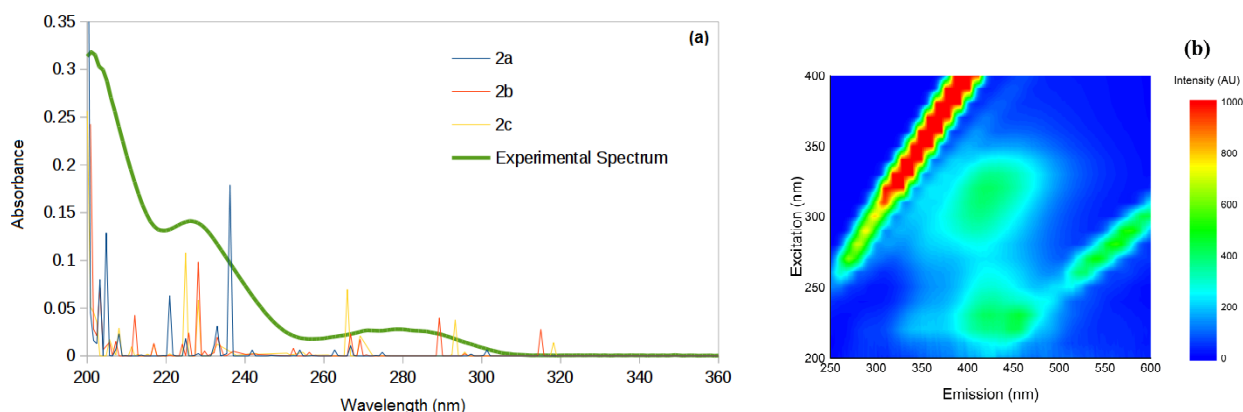
Figure 3. a) **Experimental absorption spectrum of 0.1 mM 4PP and calculated transitions. b) EEM matrix of 0.1 mM 4PP in aqueous solution.**

3.3. 4-(4-Phenoxy)phenoxyphenol (4PPP)

In the case of the three-ring system 4PPP, three conformers (3a, 3b, 3c) were found. They are described by the dihedral angles between the three aromatic rings (each conformer is described by a total of four dihedral angles). The structures of 3a, 3b and 3c are reported in the SM, and the predicted order of stability and abundance is 3a > 3c ~ 3b. As before, eighty absorption transitions were calculated for each conformer and the main ones are reported in Figure 4. When considering the band broadening that is expected to take place in aqueous solution, one may predict that 4PPP would absorb radiation below 340 nm and that the identity/structure of the absorption bands would be partially lost (see Figure SM8 in the SM).
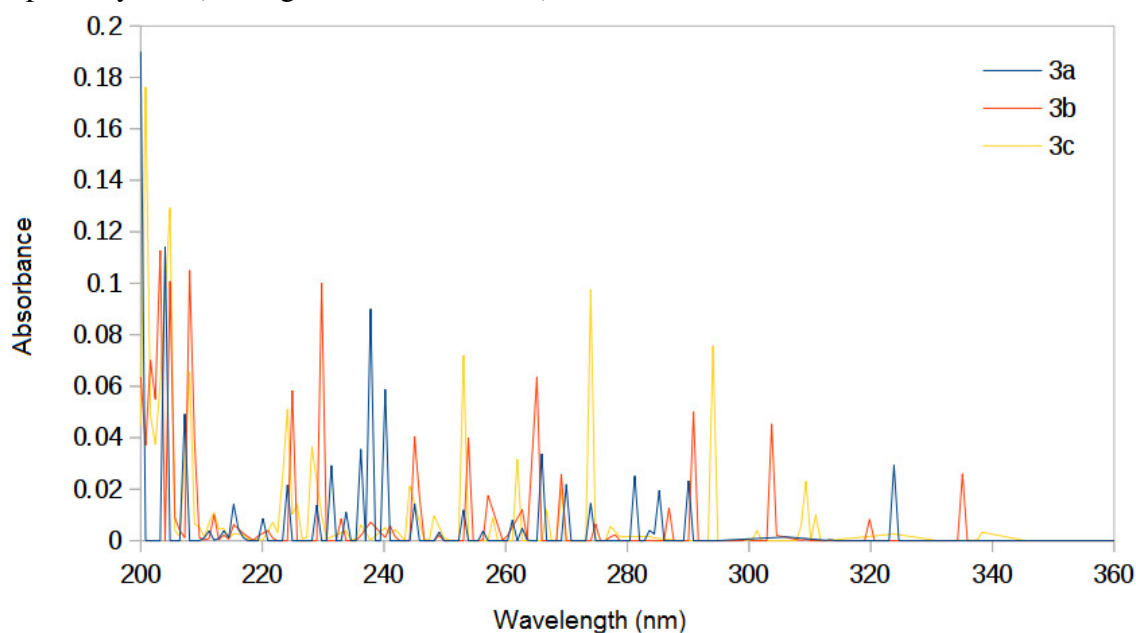
Figure 4. Calculated absorption transitions of 4PPP.

A S_1 state can be computed for each ground-state conformer, from which it mainly differs for the values of the dihedral angles (see the SM for the structures of $3aS_1$, $3bS_1$ and $3cS_1$). Interestingly, similar emission wavelengths (in the 447-448 nm range) are predicted for the three $S_1 \to S_0$ transitions. Coherently with this fact, we can observe that all three transitions are due to an electron transfer from the π framework of the phenol moiety to the π framework of the adjacent phenoxyl moiety (Figure SM4). Therefore, 4PPP would emit fluorescence radiation around 450 nm.

3.4. 4-(4-(4-Phenoxy)phenoxy)phenoxyphenol (4PPPP).

The four-ring system 4PPPP has six different stable conformers (4a-4f, see SM) with comparable abundance, a partial exception being 4f that is the least stable. The conformers differ for the six dihedral angles between the aromatic rings. The absorption transitions of 4PPPP were derived with the usual procedure and they are shown in Figure 5. The large number of transitions covers with regularity the wavelength range up to at least 360 nm. Under these circumstances, the simulated absorption spectrum of 4PPPP would show an overall decrease of the absorption intensity with increasing wavelength, with limited spectral features (see Figure SM9 in the SM). It might be tempting to draw a parallel between such condition and the featureless pseudo-exponential decay with wavelength that is observed in the absorption spectra of humic substances in surface waters and of atmospheric HULIS [54,55]. However, the absorption spectra of humic compounds are thought to originate from inter-molecular charge-transfer interactions and not from molecular chromophores [55].

Similarly to 4PP and 4PPP, also in the case of 4PPPP the S1 conformers (4aS1-4fS1, see the SM) mainly differ for the dihedral angles. The predicted emission wavelengths for five of the conformers are very similar and range from ~446 to ~448 nm. For a sixth conformer (4b) the calculated emission wavelength is 434 nm.
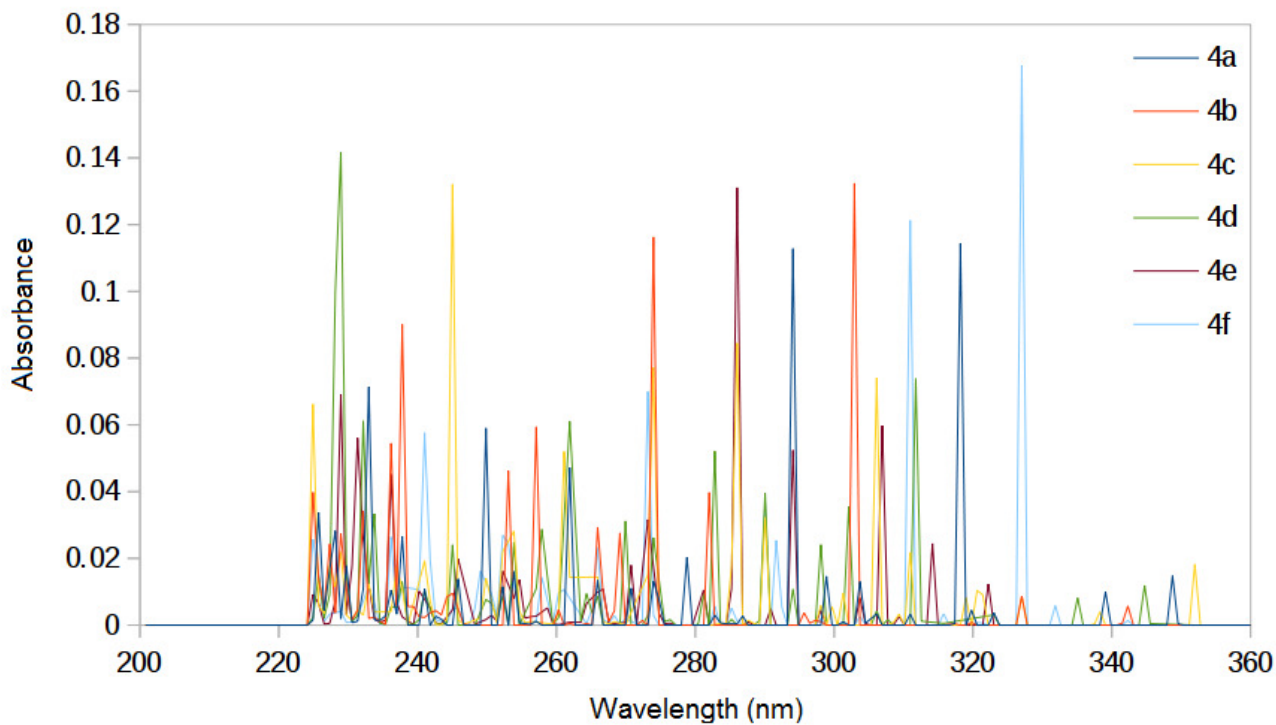
Figure 5. Calculated absorption transitions of 4PPPP.

3.5. Trends of the fluorescence emission wavelengths

The calculated wavelengths of fluorescence emission are in good or very good agreement with the experimental data, when available (phenol and 4PP). Moreover, computational results predict an increase of the fluorescence emission wavelengths with increasing number of aromatic rings, which is shown in Figure 6.
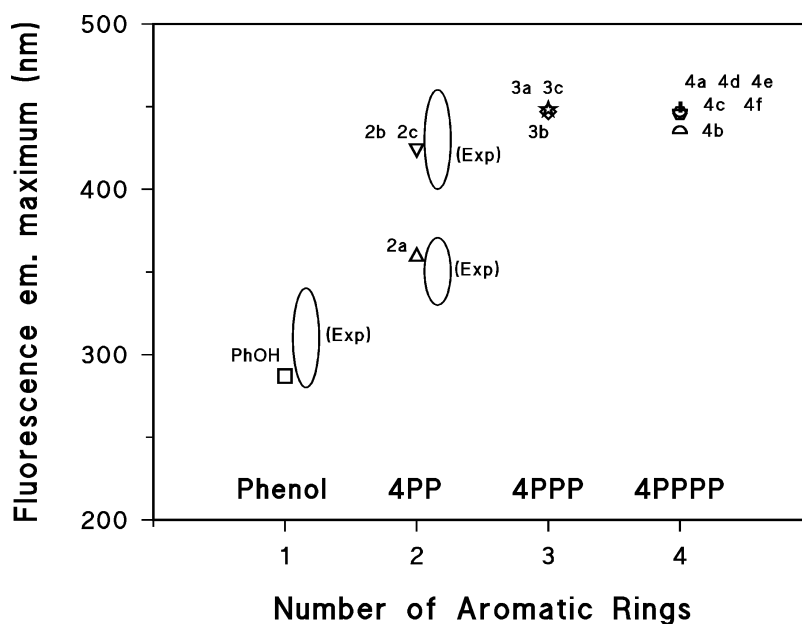
Figure 6. Trend of the calculated fluorescence emission maxima of the investigated compounds (their different conformers are indicated on the plot), as a function of the number of aromatic rings. The experimental data (Exp: wavelength range of the measured emission band) for phenol and 4PP are also reported as ellipses near the relevant calculation results.

4PP was the only case where two considerably different emission wavelengths were predicted for the various conformers. Both emissions were actually observed in the experimental spectrum, although the emission corresponding to conformer 2a was much weaker than the other one (2b + 2c). Note that the conformer 2b would be the most stable and, therefore, the most abundant.

The trend reported in Figure 6 shows a plateau in the calculated fluorescence emission maxima near 450 nm, and there is very little difference between the emission wavelengths predicted for 4PPP and 4PPPP. This trend is confirmed by the emission at 444 nm calculated for one conformer of the five-ring system 4-(4-(4-(4-phenoxy)phenoxy)phenoxy)phenoxyphenol (4PPPPP), which is almost identical to the emission from 4PPPP. This issue can be reasonably explained when taking into account the nature of the excited states, looking at the differential electronic densities. From the graphical representation of the differential electronic density (Figure 7 reports the differential electronic density map for the conformer 4d of 4PPPP, the maps for the other conformers are reported in the SM), one can deduce that the excited states (S_1) of the molecules with two or more rings show a charge-transfer (CT) character. All pictures show an electron transfer from the π orbitals of one aromatic ring to the π orbitals of a different aromatic ring (with some participation of the p orbitals on the oxygen atoms). In particular, for all the molecules with calculated fluorescence around 446-448 nm (4PPPPP, five out of six conformers of 4PPPP and all the three conformers of

4PPP), the electronic transfer is from the first aromatic ring (that bearing the hydroxyl group) to the second or the third aromatic ring. By contrast, the 434 nm emission from conformer 4b corresponds to a CT from the third to the second ring. For 4PP, the excited states emitting at 425 nm (2b and 2c) correspond to a CT from the first ring to the second, while the conformer emitting at 359 nm (2a) corresponds to a CT from the second ring to the first.
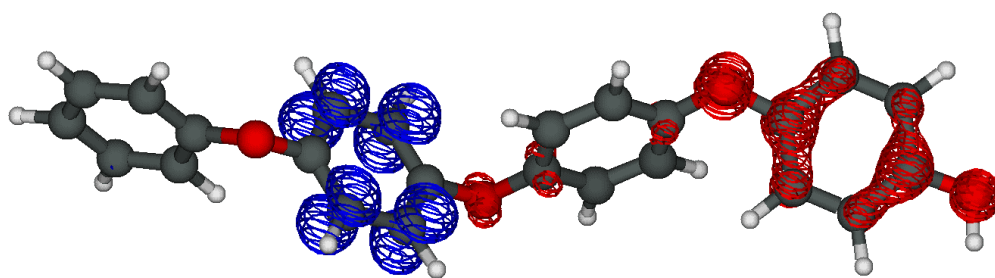
Figure 7. Differential electronic density map between the states S_1 and S_0 in conformer 4d of 4PPPP.

It is interesting to point out that the predicted emission at ~450 nm is well within the fluorescence region of HULIS [4], and it is also very near the fluorescence signal observed upon phototransformation of phenolic compounds, under conditions where the formation of phenoxy radicals and the subsequent dimerization/oligomerization processes are quite likely [23,56]. The computational results presented here give support to the hypothesis that the observed fluorescence is accounted for by phenol oligomers: an ongoing oligomerization process, with formation of progressively larger systems with an increasing number of aromatic rings, would produce a fluorescence signal at wavelengths approaching 450 nm. At that point, the possible formation of larger compounds is not expected to cause an important modification of the emission wavelengths.

Another interesting issue concerns the absorption spectra, where a gradual shift of the absorption towards higher wavelengths is predicted for the oligomers with more aromatic rings, together with a loss of the individual features of the different bands. An absorbance increase at higher wavelengths has been reported under conditions where oligomerization is operational, both in gas-solid systems and in solution, together with the appearance of a featureless decay of the absorption with increasing wavelength [22,56]. However, differently from the case of phenol oligomers, the experimental absorption was extended into the visible, which is most likely due to charge-transfer bands caused by interaction between electron donors and acceptors. Donors and acceptors might include phenols and aromatic carbonyls, respectively, that could be formed under oxidative conditions. The acceptor-donor inter-molecular interactions would be characterized by

efficient processes of internal conversion, with an efficient quenching of the possible fluorescence emission [55]. Therefore, phenol oligomers could account for the observed fluorescence emission, but their contribution to the experimental absorption spectra is expectedly limited.

4. Conclusions

Phenol dimers and oligomers are characterized by the presence of different conformers, which differ for the dihedral angles between the aromatic rings. Each conformer gives its own contribution to the absorption and fluorescence spectra of the investigated compounds. In particular, 4PP and 4PPP have three stable conformers each, while 4PPPP has six conformers. The predicted wavelengths of fluorescence emission, which correspond to $S_1 \rightarrow S_0$ transitions, increase up to a plateau when increasing the number of aromatic rings. Considering that the transitions producing fluorescence involve at most three aromatic rings, important changes in the emission wavelength are not expected when further increasing the molecular size. This issue is further supported by the calculated fluorescence emission of one of the conformers of 4PPPPP.

The plateau in the predicted emission wavelengths is at around 450 nm, which is quite in the fluorescence range of HULIS. The oligomeric compounds might thus account for the HULIS-type fluorescence, which has been observed under conditions where phenol oligomerization was operational due to the formation of phenoxy radicals [23]. Interestingly, the plateau in the emission wavelengths predicts that a mixture of phenol oligomers could not show fluorescence in a different spectral interval than the one that is experimentally observed: the increasing molecular size would initially shift fluorescence from the phenolic region to the HULIS one, but further increases of the ring number are not expected to produce important modifications in the wavelengths of the emission signal.

References

[1] E. Dinar, I. Taraniuk, E.R. Graber, S. Katsman, T. Moise, T. Anttila, T.F. Mentel, Y. Rudich, Cloud Condensation Nuclei properties of model and atmospheric HULIS, Atmos. Chem. Phys. 6 (2006) 2465-2482.

[2] A. Hoffer, A. Gelencsér, P. Guyon, G. Kiss, O. Schmid, G.P. Frank, P. Artaxo, M.O. Andreae, Optical properties of humic-like substances (HULIS) in biomass-burning aerosols, Atmos. Chem. Phys. 6 (2006) 3563-3570.

[3] T.B. Kristensen, N.L. Prisle, M. Bilde, Cloud droplet activation of mixed model HULIS and NaCl particles: Experimental results and κ-Köhler theory, Atmos. Res. 137 (2014) 167-175.

[4] E.R. Graber, Y. Rudich, Atmospheric HULIS: How humic-like are they? A comprehensive and critical review, Atmos. Chem. Phys. 6 (2006) 729-753.

[5] S. Decesari, M.C. Facchini, E. Matta, M. Mircea, S. Fuzzi, A.R. Chughtai, D M. Smith, Water-soluble organic compounds formed by oxidation of soot, Atmos. Environ. 36 (2002) 1827-1832.

[6] I. Salma, R. Ocskay, X.G. Chi, W. Maenhaut, Sampling artefacts, concentration and chemical composition of fine water-soluble organic carbon and humic-like substances in a continental urban atmospheric environment, Atmos. Environ. 41 (2007) 4106-4118.

[7] M. Paglione, A. Kiendler-Scharr, A.A. Mensah, E. Finessi, L. Giulianelli, S. Sandrini, M.C. Facchini, S. Fuzzi, P. Schlag, A. Piazzalunga, E. Tagliavini, J.S. Henzing, S. Decesari, Identification of humic-like substances (HULIS) in oxygenated organic aerosols using NMR and AMS factor analyses and liquid chromatographic techniques. Atmos. Chem. Phys. 14 (2014) 25-45.

[8] B.R.T. Simoneit, Eolian particulates from oceanic and rural areas – Their lipids, fulvic and humic acids and residual carbon, in: Advances in Organic Geochemistry. A. G. Douglas and J. R. Maxwell (eds.), Pergamon Press, Oxford, 1980, 343-352.

[9] N. Calace, B.M. Petronio, R. Cini, A.M. Stortini, B. Pampaloni, R. Udisti, Humic marine matter and insoluble materials in Antarctic snow, Intern. J. Environ. Anal. Chem. 79 (2001) 331-348.

[10] E.O. Fors, J. Rissler, A. Massling, B. Svenningsson, M.O. Andreae, U. Dusek, G.P. Frank, A. Hoffer, M. Bilde, G. Kiss, S. Janitsek, S. Henning, M.C. Facchini, S. Decesari, E. Swietlicki, Hygroscopic properties of Amazonian biomass burning and European background HULIS and investigation of their effects on surface tension with two models linking H-TDMA to CCNC data, Atmos. Chem. Phys. 10 (2010) 5625-5639.

[11] G.J. Zheng, K.B. He, F.K. Duan, Y. Cheng, Y.L. Ma, Measurement of humic-like substances in aerosols: A review, Environ. Pollut. 181 (2013) 301-314.

[12] M.P. Tolocka, M. Jang, J.M. Ginter, F.J. Cox, R.M. Kamens, M.V. Johnston, Formation of oligomers in secondary organic aerosol, Environ. Sci. Technol. 38 (2004) 1428-1434.

[13] A. Cappiello, E. De Simoni, C. Fiorucci, F. Mangani, P. Palma, H. Trufelli, S. Decesari, M.C. Facchini, S. Fuzzi, Molecular characterization of the water-soluble organic compounds in fogwater by ESIMS/MS, Environ. Sci. Technol. 37 (2003) 1229-1240.

[14] R.M.B.O. Duarte, C.A. Pio, A.C. Duarte, Spectroscopic study of the water-soluble organic matter isolated from atmospheric aerosols collected under different atmospheric conditions, Anal. Chim. Acta 530 (2005) 7-14.

[15] R.M.B.O. Duarte, A.C. Duarte, A critical review of advanced analytical techniques for water-soluble organic matter from atmospheric aerosols, Trac - Trends Anal. Chem. 30 (2011) 1659-1671.

[16] O. Laskina, M.A. Young, P.D. Kleiber, V.H. Grassian, Infrared optical constants of organic aerosols: Organic acids and model humic-like substances (HULIS), Aerosol Sci. Technol. 48 (2014) 630-637.

[17] C.L. Muller, C. Kidd, I.J. Fairchild, A. Baker, Investigation into clouds and precipitation over an urban area using micro rain radars, satellite remote sensing and fluorescence spectrophotometry, Atmos. Res. 96 (2010) 241-255.

[18] R.G. Pinnick, E. Fernandez, J.M. Rosen, S.C. Hill, Y. Wang, Y.L. Pan, Fluorescence spectra and elastic scattering characteristics of atmospheric aerosol in Las Cruces, New Mexico, USA: Variability of concentrations and possible constituents and sources of particles in various spectral clusters, Atmos. Environ. 65 (2013) 195-204.

[19] S. Net, L. Nieto-Gligorovski, S. Gligorovski, B. Temime-Rousell, S. Barbati, Y.G. Lazarou, H. Wortham, Heterogeneous light-induced ozone processing on the organic coatings in the atmosphere, Atmos. Environ. 43 (2009) 1683-1692.

[20] S. Net, E. Gómez Alvarez, S. Gligorovski, H. Wortham, Heterogeneous reactions of ozone with methoxyphenols, in presence and absence of light, Atmos. Environ. 45 (2011) 3007-3014.

[21] L. Nieto-Gligorovski, S. Net, S. Gligorovski, C. Zetzsch, A. Jammoul, B. D'Anna, C. George, Interactions of ozone with organic surface films in the presence of simulated sunlight: Impact on wettability of aerosols, Phys. Chem. Chem. Phys. 10 (2008) 2964-2971.

[22] L. Nieto-Gligorovski, S. Net, S. Gligorovski, H. Wortham, H. Grothe, C. Zetzsch, Spectroscopic study of organic coatings on fine particles, exposed to ozone and simulated sunlight, Atmos. Environ. 44 (2010) 5451-5459.

[23] E. De Laurentiis, B. Sur, M. Pazzi, V. Maurino, C. Minero, G. Mailhot, M. Brigante, D. Vione, Phenol transformation and dimerisation, photosensitised by the triplet state of 1-nitronaphthalene: A possible pathway to humic-like substances (HULIS) in atmospheric waters, Atmos. Environ. 70 (2013) 318-327.

[24] J. P. Aguer, C. Richard, Photochemical behaviour of humic acid synthesized from phenol, J. Photochem. Photobiol. A: Chem. 84 (1994) 69-73.

[25] D. Vione, V. Maurino, C. Minero, Photosensitised humic-like substances (HULIS) formation processes of atmospheric significance: A review, Environ. Sci. Pollut. Res. 21 (2014) 11614-11622.

[26] P.G. Coble, Characterization of marine and terrestrial DOM in seawater using excitation–emission spectroscopy, Mar. Chem. 51 (1996) 325-346.

[27] S.K.L. Ishii, T.H. Boyer, Behavior of reoccurring PARAFAC components in fluorescent dissolved organic matter in natural and engineered systems: A critical review. Environ. Sci. Technol. 46 (2012) 2006-2017.

[28] F. Jensen, Introduction to Computational Chemistry, John Wiley & Sons, NY, 1999, ISBN 0-471-98425-98426.

[29] R.G. Parr, W. Yang, Density Functional Theory of Atoms and Molecules, Oxford University Press, 1989.

[30] W. Kohn, A.D. Becke, R.G. Parr, Density functional theory of electronic structure, J. Phys. Chem. 100 (1996) 12974-12980.

[31] R. Bauernschmitt and R. Ahlrichs, Treatment of electronic excitations within the adiabatic approximation of time dependent density functional theory, Chem. Phys. Lett. 256 (1996) 454-464.

[32] A. Dreuw, M. Head-Gordon, Single-reference ab initio methods for the calculation of excited states of large molecules, Chem. Rev. 105 (2005) 4009-4037.

[33] D. Jacquemin, E.A. Perpète, O.A. Vydrov, G.E. Scuseria, C. Adamo, Assessment of long-range corrected functionals performance for n→π* transitions in organic dyes, J. Chem. Phys. 127 (2007) 094102.

[34] D. Jacquemin, V. Wathelet, E.A. Perpète, C. Adamo, Extensive TD-DFT benchmark: Singlet-excited states of organic molecules, J. Chem. Theory Comput. 5 (2009) 2420-2435.

[35] A. D. Laurent, D. Jacquemin, TD-DFT Benchmarks: A Review, Int. J. Quantum Chem. 113 (2013) 2019–2039.

[36] B. Mennucci, J. Tomasi, Continuum solvation models: a new approach to the problem of solute's charge distribution and cavity boundaries, J. Chem. Phys. 106 (1997) 5151-5158.

[37] M. Cossi, N. Rega, G. Scalmani, V. Barone, Polarizable dielectric model of solvation with inclusion of charge penetration effects, J. Chem. Phys. 114 (2001) 5691-5570.

[38] A.V. Marenich, C.J. Cramer, D.G. Truhlar, Universal solvation model based on solute electron density and on a continuum model of the solvent defined by the bulk dielectric constant and atomic surface tensions, J. Phys. Chem. B 113 (2009) 6378–6396.

[39] A.V. Marenich, C.J. Cramer, D.G. Truhlar, Performance of SM6, SM8, and SMD on the SAMPL1 test set for the prediction of small-molecule solvation free energies, J. Phys. Chem. B 113 (2009) 4538-4543.

[40] C. Adamo, V. Barone, Exchange functionals with improved long-range behavior and adiabatic connection methods without adjustable parameters: The mPW and mPW1PW models, J. Chem. Phys. 108 (1998) 664-675.

[41] C. Lee, W. Yang, R.G. Parr, Development of the Colle-Salvetti correlation-energy formula into a functional of the electron density, Phys. Rev. B 37 (1988) 785-789.

[42] B. Miehlich, A. Savin, H. Stoll, H. Preuss, Results obtained with the correlation-energy density functionals of Becke and Lee, Yang and Parr, Chem. Phys. Lett. 157 (1989) 200-206.

[43] W.J. Hehre, R. Ditchfield, J.A. Pople, Self-consistent molecular orbital methods. XII. Further extensions of Gaussian-type basis sets for use in molecular orbital studies of organic molecules, J. Chem. Phys. 56 (1972) 2257-2261.

[44] T. Clark, J. Chandrasekhar, G.W. Spitznagel, P.v.R. Schleyer, Efficient diffuse function-augmented basis-sets for anion calculations. 3. The 3-21+G basis set for 1st-row elements, Li-F, J. Comput. Chem. 4 (1983) 294-301.

[45] M.J. Frisch, G.W. Trucks, H.B. Schlegel, G.E. Scuseria, M.A. Robb, J.R. Cheeseman, G. Scalmani, V. Barone, B. Mennucci, G.A. Petersson, H. Nakatsuji, M. Caricato, X. Li, H. P. Hratchian, A.F. Izmaylov, J. Bloino, G. Zheng, J.L. Sonnenberg, M. Hada, M. Ehara, K. Toyota, R. Fukuda, J. Hasegawa, M. Ishida, T. Nakajima, Y. Honda, O. Kitao, H. Nakai, T. Vreven, J.A. Montgomery Jr., J.E. Peralta, F. Ogliaro, M. Bearpark, J.J. Heyd, E. Brothers, K.N. Kudin, V.N. Staroverov, R. Kobayashi, J. Normand, K. Raghavachari, A. Rendell, J.C. Burant, S.S. Iyengar, J. Tomasi, M. Cossi, N. Rega, J.M. Millam, M. Klene, J.E. Knox, J.B. Cross, V. Bakken, C. Adamo, J. Jaramillo, R. Gomperts, R.E. Stratmann, O. Yazyev, A.J. Austin, R. Cammi, C. Pomelli, J.W. Ochterski, R.L. Martin, K. Morokuma, V.G. Zakrzewski, G.A. Voth, P. Salvador, J.J. Dannenberg, S. Dapprich, A.D. Daniels, Ö. Farkas, J.B. Foresman, J.V. Ortiz, J. Cioslowski, D.J. Fox, Gaussian 09, Gaussian, Inc., Wallingford, CT, 2009.

[46] G. Schaftenaari, J.H. Noordik, Molden: a pre- and post-processing program for molecular and electronic structures, J. Comput.-Aided Mol. Des. 14 (2000) 123-134.

[47] N.J. Turro, V. Ramamurthy, W. Cherry, W. Farneth, The effect of wavelength on organic photoreactions in solution. Reactions from upper excited states, Chem. Rev. 78 (1978) 125-145.

[48] D. B. Jones, G. B. da Silva, R. F. C. Neves, H. V. Duque, L. Chiari, E. M. de Oliveira, M. C. A. Lopes, R. F. da Costa, M. T. do N. Varella, M. H. F. Bettega, M. A. P. Lima and M. J. Brunger, An experimental and theoretical investigation into the excited electronic states of phenol, J. Chem. Phys. 141 (2014) 074314.

[49] R. A. Livingstone, J. O. F. Thompson, M. Iljina, R. J. Donaldson, B. J. Sussman, M. J. Paterson, and D. Towsend, Time-resolved photoelectron imaging of excited state relaxation dynamics in phenol, catechol, resorcinol, and hydroquinone, J. Chem. Phys. 137 (2012) 184304.

[50] O. P. J. Vieuxmaire, Z. Lan, A. L. Sobolewski, and W. Domcke, Ab initio characterization of the conical intersections involved in the photochemistry of phenol, J. Chem. Phys. 129 (2008) 224307.

[51] L. Zhang, G. H. Peslherbe and H. M. Muchall, Ultraviolet Absorption Spectra of Substituted Phenols: A Computational Study, Photochem. Photobiol. 82 (2006) 324-331.

[52] C. Ratzer, J. Kupper, D. Spangenberg and Michael Schmit, The structure of phenol in the S1-state determined by high resolution UV-spectroscopy, Chem. Phys. 283 (2002) 153–169.

[53] N. W. Larsen, Microwave spectra of the six mono-carbon-13-substituted phenols and of some monodeuterated species of phenol. Complete substitution structure and absolute dipole moment, J. Mol. Struct. 51 (1979) 175-190.

[54] A. Albinet, C. Minero, D. Vione, Photochemical generation of reactive species upon irradiation of rainwater: Negligible photoactivity of dissolved organic matter, Sci. Total Environ. 408 (2010) 3367-3373.

[55] C.M. Sharpless, N.V. Blough, The importance of charge-transfer interactions in determining chromophoric dissolved organic matter (CDOM) optical and photochemical properties, Environ. Sci.: Processes Impacts 16 (2014) 654-671.

[56] A. Bianco, M. Minella, E. De Laurentiis, V. Maurino, C. Minero, D. Vione, Photochemical generation of photoactive compounds with fulvic-like and humic-like fluorescence in aqueous solution, Chemosphere 111 (2014) 529-536.

SUPPLEMENTARY MATERIAL

Computational assessment of the fluorescence emission of phenol oligomers: A possible insight into the fluorescence properties of humic-like substances (HULIS).

Francesco Barsotti,[a] Giovanni Ghigo,[b],* Davide Vione [a],*

Dipartimento di Chimica, Università di Torino Via Giuria 5[a] and/or 7[b], 10125 Torino, Italy.

* Address correspondence to either author: *giovanni.ghigo@unito.it* (G. Ghigo, Phone +39-011-6707872), *davide.vione@unito.it* (D. Vione, Phone +39-011-6705296)

1.   Benchmark study

2.   Optimized structures

   4-Phenoxyphenol (4PP)

   4-(4-Phenoxy)phenoxyphenol (4PPP)

   4-(4-(4-Phenoxy)phenoxy)phenoxyphenol (4PPPP)

3.   Weight function and simulated spectra

4.   References

1. Benchmark study

The aim of the benchmark phase was to identify the proper combination of functional/basis set that could best describe the system, minimizing the calculation time but still allowing a good accuracy. All the benchmark tests were carried out using phenol as sample molecule. Every functional-basis set couple was used to optimize the geometry and calculate the absorption energy, within TD-DFT.

The nature of the critical points was checked by vibrational analysis, and absorption was calculated just on minimums. The first step of this work was the choice of the basis set, using two different functionals. The results showed that the basis set is not so important because absorption does not change significantly when the basis set is modified. Because the larger basis sets make the calculation time longer and because the present work involves the study of rather large phenol oligomers, the chosen basis was the one that allowed the fastest calculations.

The second step was the choice of the functional. After trying with some couples of combination and exchange algorithms, the final choice involved the couple giving UV-visible absorption that was nearer to the experimental data (phenol absorption spectrum in water, obtained by spectrophotometric measurements with a Varian Cary 100 Scan instrument using quartz cuvettes with 1 cm path length). The final goal was to simulate fluorescence. In agreement with Kasha's rule (Kasha, 1950), the considered transition in the choice of the functional-basis set couple, to be compared with experiment, was the one with the lowest energy. The absorption of radiation that is observed experimentally in the condensed phase (solution) shows rather large bands, while the calculations give a single value that would coincide with the maximum of the band. Phenol absorption in the UV-Visible range has two main peaks, one around 270 nm and another around 210 nm. The latter absorption peak is common to all aromatic compounds that show a similar behaviour in the relevant spectral region. Therefore, this work was focused on the low-energy transition (~270 nm), which is peculiar of phenol and which could approach the visible range within the studied oligomers.

The functionals BLYP and PBEhPBE were tested with two Pople's basis sets (6-31+G(d) and 6-311+G(d,p)) and with two correlation-consistent basis sets (Cc-pVTZ and Aug-Cc-pVTZ). A minimal variation of the calculated transition energy was achieved with a considerable increase of the calculation time, thus the Pople's basis sets were chosen.

Other eight functionals were tested with these two basis sets. Considering the small variations of the predicted signal and the differences in calculation time, other seven functionals were additionally tested just with the smaller Pople's basis set.

After the screening it was decided to use the mPWLYP functional (modified Perdew-Wang exchange functional and Lee-Yang-Parr correlation) with the Pople basis set 6-31+G(d), because this method gives a suitable approximation of the experimental values and requires reasonable calculation time.

The following chart reports the results obtained with the different combinations of functionals and basis sets.

Functional	Basis Set	λ_1 (nm)	λ_2 (nm)	λ_3 (nm)	λ_4 (nm)	λ_5 (nm)	f_1	f_2	f_3	f_4	f_5
BLYP	6-31+G(d)	263.14	234.05	226.21	222.20	208.43	0.0395	0.0000	0.0762	0.0032	0.0004
	6-311+G(d,p)	263.69	232.48	226.48	220.13	208.47	0.0376	0.0005	0.0786	0.0034	0.0004
	Cc-pVTZ	260.89	221.66	199.72	194.52	194.41	0.0404	0.0734	0.0002	0.0006	0.2817
	Aug-Cc-pVTZ	263.49	248.78	233.99	227.63	224.80	0.0373	0.0009	0.0032	0.0757	0.0004
PBEhPBE	6-31+G(d)	260.60	225.85	222.85	214.01	201.36	0.0420	0.0000	0.0889	0.0031	0.0004
	6-311+G(d,p)	261.37	224.73	223.61	212.15	200.52	0.0406	0.0005	0.0900	0.0033	0.0005
	Cc-pVTZ	259.18	219.16	193.38	192.46	188.05	0.0431	0.0827	0.0004	0.2746	0.0004
	Aug-Cc-pVTZ	261.49	238.55	224.57	223.63	214.99	0.0401	0.0009	0.0855	0.0032	0.0005
B3LYP	6-31+G(d)	244.39	214.45	213.76	201.69	190.75	0.0461	0.0000	0.0553	0.0055	0.0004
	6-311+G(d,p)	245.18	214.70	213.89	200.67	190.38	0.0455	0.0571	0.0003	0.0055	0.0004
B3PW91	6-31+G(d)	242.20	211.04	201.63	190.87	185.40	0.0475	0.0640	0.0000	0.0051	0.4985
	6-311+G(d,p)	243.01	212.03	202.40	190.71	185.81	0.0478	0.0643	0.0004	0.0053	0.5202
CAM-B3LYP	6-31+G(d)	235.89	207.00	202.28	186.73	178.81	0.0486	0.0495	0.0001	0.0078	0.0006
	6-311+G(d,p)	236.69	208.08	201.92	186.50	178.99	0.0482	0.0504	0.0001	0.0082	0.0005
mPWLYP	6-31+G(d)	263.95	248.35	233.83	226.95	221.07	0.0406	0.0000	0.0028	0.0738	0.0004
	6-311+G(d,p)	264.47	248.29	233.58	227.62	221.48	0.0394	0.0004	0.0035	0.0758	0.0005
M06	6-31+G(d)	246.56	233.75	218.96	214.61	202.24	0.0514	0.0005	0.0018	0.0004	0.0002
	6-311+G(d,p)	247.58	238.99	226.22	221.03	207.39	0.0493	0.0001	0.0029	0.0007	0.0001
M06-L	6-31+G(d)	245.11	213.38	201.85	193.44	185.80	0.0474	0.0001	0.0019	0.0002	0.0000
	6-311+G(d,p)	246.54	214.22	206.88	198.30	191.47	0.0445	0.0608	0.0005	0.0019	0.0003
M06-2X	6-31+G(d)	233.56	202.38	202.13	186.75	179.59	0.0526	0.0734	0.0005	0.0061	0.0009
	6-311+G(d,p)	233.92	203.89	203.74	189.05	181.90	0.0522	0.0650	0.0000	0.0079	0.0010
TPSS	6-31+G(d)	254.23	219.26	219.14	208.12	196.75	0.0416	0.0785	0.0000	0.0033	0.0004
	6-311+G(d,p)	254.79	220.05	218.96	207.26	196.81	0.0405	0.0790	0.0005	0.0035	0.0004
TPSSh	6-31+G(d)	245.81	213.70	211.04	199.54	189.19	0.0447	0.0684	0.0000	0.0042	0.0004
wPBEhLYP	6-31+G(d)	263.40	246.94	232.01	227.20	217.84	0.0411	0.0000	0.0035	0.0761	0.0005
wPBEhPBE	6-31+G(d)	260.62	225.54	222.86	213.99	201.34	0.0420	0.0000	0.0888	0.0031	0.0004
mPW1LYP	6-31+G(d)	242.25	223.85	208.54	198.45	195.05	0.0483	0.0001	0.0054	0.0005	0.0005
mPWPBE	6-31+G(d)	260.33	228.21	222.81	216.68	205.21	0.0416	0.0000	0.0853	0.0026	0.0003
mPWLYP	6-31+G(d)	239.07	209.24	206.82	194.06	184.92	0.0505	0.0588	0.0000	0.0052	0.0005
PBEh1PBE	6-31+G(d)	239.18	209.12	204.45	191.96	182.25	0.0505	0.0606	0.0000	0.0060	0.0005
Experimental Data		270	nm								

Basis sets used are:

- 6-31+G(d) (Petersson et al., 1988; Petersson et al., 1991)
- 6-311+G(d,p) (McLean et al., 1980; Raghavachari et al., 1980)
- Cc-pVTZ (Dunning, 1989; Kendall et al., 1992; Davidson, 1996)
- Aug-Cc-pVTZ (Dunning, 1989; Kendall et al., 1992; Davidson, 1996)

Functional used are:

- BLYP: Becke exchange functional (Becke, 1988) and the correlation functional of Lee, Yang, and Parr (Lee et al., 1988)
- PBEhPBE: exchange functional of Perdew, Burke and Ernzerhof (Perdew et al., 1996) revisioned (M. Ernzerhof et al, 1998) and the gradient corrected correlation functional of Perdew, Burke and Ernzerhof (Perdew et al., 1996; Perdew et al., 1997)
- B3LYP: Becke Three Parameter Hybrid Functionals (Becke, 1993) and the correlation functional of Lee, Yang, and Parr. (Lee et al., 1988)

- B3PW91: Becke Three Parameter Hybrid Functionals (Becke, 1993) and the gradient-corrected correlation functional of Perdew and Wang (Perdew et al., 1996; Burke et al., 1998)
- CAM-B3LYP: a long range corrected version of B3LYP using the Coulomb-attenuating method (Yanai et al., 2004; Becke, 1993; Lee et al., 1988)
- mPWLYP: Perdew-Wang 1991 exchange functional modified by Adamo and Barone (Adamo and Barone, 1998) and the correlation functional of Lee, Yang, and Parr (Lee et al., 1988)
- M06: the hybrid functional of Truhlar and Zhao (Zhao et al., 2006)
- M06-L: the pure functional of Truhlar and Zhao (Zhao et al., 2006)
- M06-2X: a variation of the hybrid functional of Truhlar and Zhao (Zhao et al., 2006)
- TPSS: the τ-dependent gradient-corrected functional of Tao, Perdew, Staroverov, and Scuseria (Tao et al., 2003)
- TPSSh: the hybrid functional using the TPSS functionals (Tao et al., 2003)
- wPBEhLYP: the exchange part of screened Coulomb potential-based final of Heyd, Scuseria and Ernzerhof (Heyd et al., 2003; Izmaylov et al., 2006; Henderson et al., 2009) and the correlation functional of Lee, Yang, and Parr (Lee et al., 1988)
- wPBEhPBE: the exchange part of screened Coulomb potential-based final of Heyd, Scuseria and Ernzerhof (Heyd et al., 2003; Izmaylov et al., 2006; Henderson et al, 2009) and the gradient corrected correlation functional of Perdew, Burke and Ernzerhof (Perdew et al, 1996; Perdew et al., 1997)
- mPW1LYP: Perdew-Wang hybrid functional exchange modified by Adamo and Barone (Adamo and Barone, 1998) and the correlation functional of Lee, Yang, and Parr. (Lee et al., 1988)
- mPWPBE: Perdew-Wang 1991 exchange functional modified by Adamo and Barone (Adamo and Barone, 1998) and the gradient corrected correlation functional of Perdew, Burke and Ernzerhof (Perdew et al., 1996; Perdew et al, 1997)
- mPWLYP: the Perdew and Wang functional exchange modified by Adamo and Barone (Adamo and Barone, 1998) and the correlation functional of Lee, Yang, and Parr. (Lee et al., 1988)
- PBEh1PBE: the hybrid functional that use a revised form of PBE pure functional (exchange and correlation) (Ernzerhof et al., 1998)

2. Optimized structures

4-Phenoxyphenol (4PP)

Differently from phenol, 4PP has three different stable conformations: two of them are very similar in energy, while the third is quite different. The main difference regards the dihedral angles between the aromatic rings. The dihedral angles are reported below (units are in degrees), together with the relevant structures.

Theta (θ) is measured considering two carbon atoms of the first aromatic ring, the oxygen and one carbon atom on the second ring. The omega (ω) angle is measured considering one carbon atom of the first ring, the oxygen and two carbon atoms of the second ring. The first ring is the one with the OH function, the other one is the second ring.
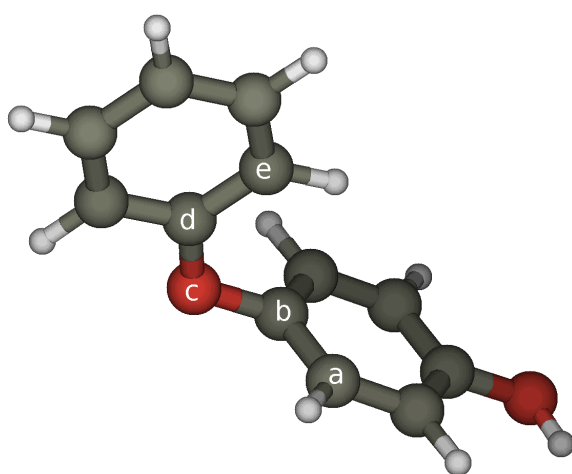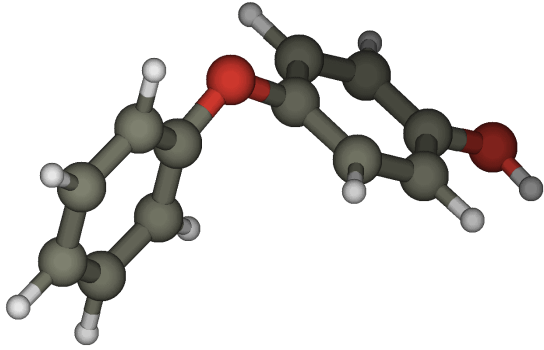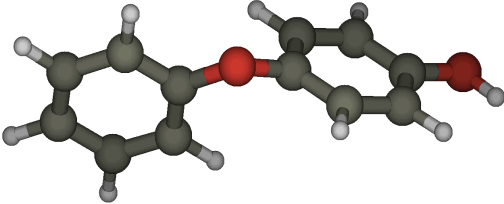
The theta (θ) angle is the one identified by a-b-c-d atoms, while omega (ω) angle is identified by b-c-d-e atoms.

Figure SM1. The 2a conformer of 4PP.
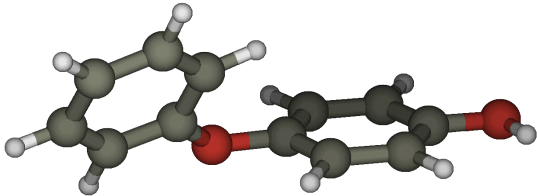
Ground State - 4PP
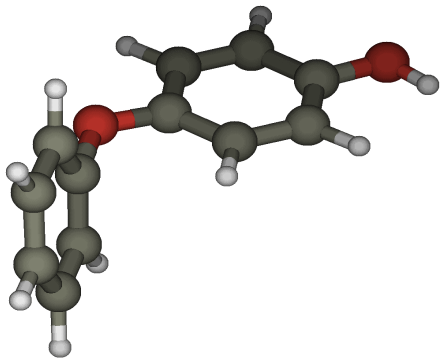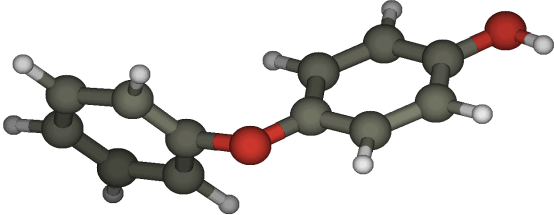
Name	Structure	(θ)	(ω)	ΔG (Kcal/mol)	Weight
2a		88	4	0.305	0.32

Name	Structure	(θ)	(ω)	ΔEnergy (Kcal/mol)	Fluorescence (nm)
2b		-61	154	0	0.53
2c		-129	-152	0.764	0.15

Excited state - 4PP

Name	Structure	(θ)	(ω)	ΔEnergy (Kcal/mol)	Fluorescence (nm)
2aS1		53	17	8.88	359

2bS1		-176	-109	0.040	425
2cS1		-4	104	0.000	425

2a	2b	2c
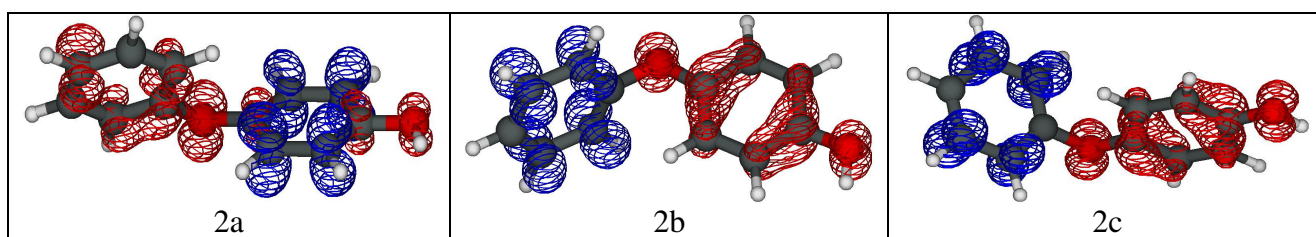
Figure SM2. Differential electronic density map between state S_1 and S_0 in the different conformations of 4PP.

The chart below shows the calculated transitions for the different conformers of 4PP (wavelengths and the force constants *f* are reported).

Calculated transitions of 2rings structures (4PP)

| 2a		2b		2c	
λ (nm)	**f**	**λ (nm)**	**f**	**λ (nm)**	f
301	0,027	315	0,028	318	0,025
297	0,007	296	0,012	296	0,021
275	0,009	289	0,105	293	0,117
273	0,001	271	0,003	272	0,001
267	0,033	269	0,024	269	0,030
263	0,023	267	0,072	266	0,075
257	0,001	258	0,001	261	0,001
254	0,008	256	0,014	255	0,021
252	0,001	252	0,024	251	0,020
247	0,005	243	0,016	243	0,003
242	0,010	243	0,005	243	0,025
242	0,001	240	0,003	239	0,001
236	0,302	237	0,005	238	0,001
235	0,016	235	0,003	237	0,003
233	0,032	233	0,020	233	0,013
232	0,017	232	0,005	231	0,008
228	0,003	230	0,014	229	0,015
227	0,004	228	0,135	228	0,080
225	0,020	226	0,078	226	0,014
222	0,004	224	0,016	225	0,118
221	0,073	221	0,001	221	0,002
221	0,000	217	0,003	217	0,015
219	0,002	217	0,014	215	0,006
214	0,004	214	0,001	214	0,003
214	0,001	213	0,010	214	0,001
213	0,001	212	0,002	213	0,002
210	0,002	212	0,043	211	0,028
208	0,024	210	0,013	210	0,004
207	0,017	207	0,030	208	0,030
206	0,000	207	0,007	207	0,002
205	0,181	206	0,129	206	0,140
205	0,031	204	0,006	206	0,018
203	0,169	203	0,150	202	0,316
202	0,042	202	0,252	202	0,215
202	0,141	202	0,060	201	0,094
201	0,083	201	0,449	200	0,257
200	0,659	198	0,150	198	0,146
197	0,031	196	0,005	196	0,027
197	0,026	196	0,003	196	0,090
196	0,034	195	0,179	195	0,008
196	0,007	195	0,022	195	0,108
195	0,049	194	0,038	194	0,015
194	0,144	194	0,009	194	0,050
193	0,054	193	0,024	193	0,022
192	0,103	193	0,046	192	0,021
191	0,007	191	0,016	191	0,001
191	0,026	189	0,022	190	0,016
188	0,012	189	0,016	189	0,018
188	0,006	188	0,016	189	0,016
187	0,002	188	0,001	189	0,026
186	0,001	187	0,004	187	0,001
185	0,003	186	0,009	186	0,127
184	0,010	186	0,106	185	0,011
184	0,000	184	0,082	184	0,021
183	0,000	184	0,002	184	0,083
183	0,002	183	0,017	183	0,001
182	0,020	181	0,000	181	0,003
181	0,003	180	0,001	180	0,006
180	0,003	180	0,010	180	0,003
180	0,001	179	0,009	179	0,014
179	0,008	179	0,039	178	0,003
178	0,040	178	0,001	178	0,011
177	0,003	178	0,003	178	0,003
177	0,006	177	0,001	178	0,019
177	0,007	177	0,005	177	0,005
176	0,010	176	0,004	177	0,001
176	0,032	176	0,004	176	0,004
175	0,017	175	0,025	175	0,007

4-(4-Phenoxy)phenoxyphenol (4PPP)

For this molecule, three different stable conformational isomers have been found. In this case as well, the difference among the optimized structures concerns the dihedral angles between the aromatic rings. The name of these angles is the same as that used for 4PP, with the difference that θ' and ω' represent the angles between the second and the third rings.
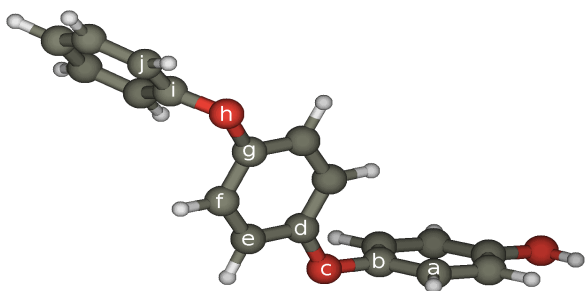
The theta (θ) angle is identified by atoms a-b-c-d, omega (ω) is identified by atoms b-c-d-e, theta' (θ') is identified by atoms f-g-h-i, and omega' (ω') is identified by atoms g-h-i-j.

Figure SM3. The 3a conformer of 4PPP.

| Name	(θ)	(ω)	(θ')	(ω')	ΔG (Kcal/mol)	Weights
3a	88	4	117	165	0	0.47
3b	-123	-159	-66	-20	0.607	0.25
3c	-60	159	129	156	0.513	0.28

Table SM1. *Structure parameters and relative free energies of the 4PPP conformers.*

Name	(θ)	(ω)	(θ')	(ω')	ΔEnergy (Kcal/mol)	Fluorescence (nm)
3aS1	3	83	117	162	0,071	447
3bS1	-3	97	69	163	0,024	448
3cS1	117	-106	-67	162	0	448

Table SM2. *Structure parameters, relative electronic energies and emission wavelengths of the 4PPP excited state conformers*

The pictures in the next page report the structures of the ground (3x) and excited states (3xS1) of the three conformers of 4PPP.

3a	3aS1
3b	3bS1
3c	3cS1

3a	3b	3c
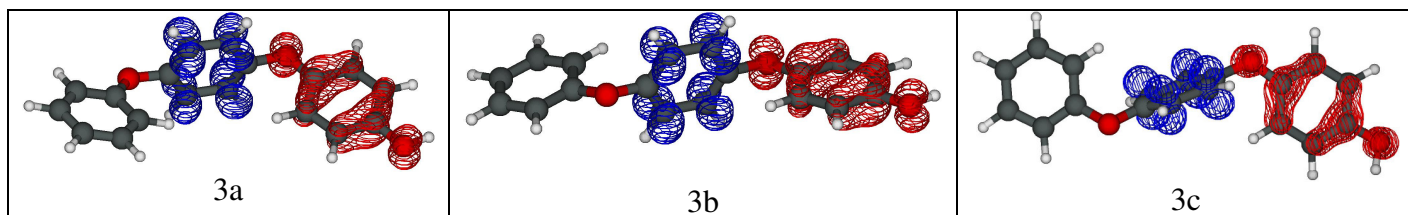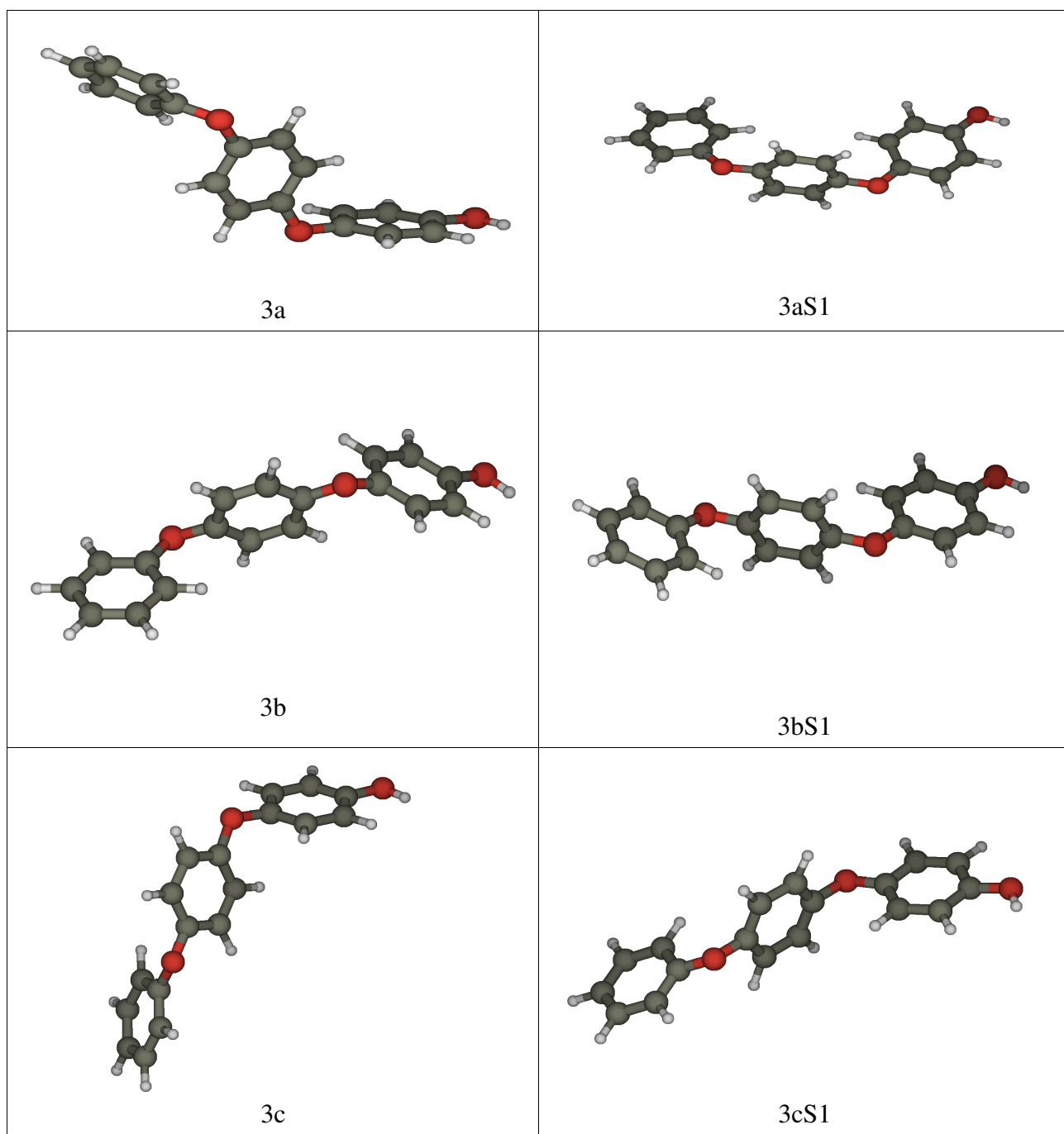
**Figure SM4.** Differential electronic density map between state S_1 and S_0 in the different conformations of 4PPP.

The chart below shows the calculated transitions for the different conformers of 4PPP (wavelengths and the force constants *f* are reported).

Calculated transitions for 3 rings structures

3a		3b		3c	
λ (nm)	f	λ (nm)	f	λ (nm)	f
324	0,050	335	0,029	338	0,013
313	0,003	320	0,016	324	0,004
306	0,002	309	0,004	311	0,010
296	0,001	304	0,161	309	0,158
290	0,024	300	0,003	301	0,017
289	0,001	291	0,070	294	0,082
285	0,044	287	0,020	288	0,002
284	0,041	284	0,001	284	0,017
281	0,050	278	0,002	279	0,003
274	0,015	277	0,003	277	0,010
270	0,023	275	0,015	274	0,099
269	0,000	269	0,010	271	0,001
267	0,026	269	0,026	269	0,028
266	0,037	265	0,082	267	0,038
263	0,018	263	0,045	262	0,036
262	0,000	260	0,008	259	0,013
261	0,010	257	0,020	258	0,004
257	0,000	256	0,001	258	0,007
256	0,013	256	0,000	254	0,002
253	0,013	254	0,053	253	0,077
250	0,002	252	0,012	251	0,002
249	0,004	249	0,002	250	0,002
248	0,001	248	0,001	248	0,025
245	0,010	246	0,027	247	0,003
245	0,004	245	0,041	244	0,047
241	0,001	242	0,003	242	0,001
240	0,112	241	0,006	242	0,007
239	0,004	240	0,002	241	0,003
238	0,034	240	0,000	240	0,005
238	0,149	238	0,013	240	0,003
237	0,006	238	0,001	240	0,002
237	0,005	238	0,001	238	0,001
236	0,060	236	0,000	236	0,010
235	0,018	236	0,003	235	0,005
234	0,023	233	0,009	234	0,009
234	0,003	232	0,014	231	0,012
231	0,140	231	0,002	230	0,014
231	0,084	230	0,250	230	0,012
230	0,016	230	0,025	229	0,018
229	0,015	229	0,003	229	0,006
228	0,011	228	0,048	228	0,050
228	0,001	226	0,018	227	0,008
225	0,007	226	0,003	226	0,046
224	0,022	225	0,064	225	0,011
224	0,002	224	0,004	224	0,049
224	0,003	224	0,039	224	0,016
223	0,010	222	0,003	223	0,121
222	0,001	222	0,001	222	0,022
221	0,007	221	0,002	222	0,006
220	0,010	221	0,003	220	0,000
219	0,005	219	0,007	218	0,002
217	0,001	217	0,002	217	0,001
217	0,001	217	0,002	217	0,002
216	0,005	215	0,014	216	0,003
215	0,048	215	0,007	215	0,010
214	0,005	214	0,013	214	0,027
214	0,017	213	0,001	213	0,003
213	0,001	212	0,005	213	0,003
213	0,001	212	0,006	212	0,005
212	0,000	211	0,002	212	0,007
211	0,011	210	0,007	211	0,020
210	0,028	209	0,001	210	0,038
209	0,003	209	0,057	209	0,010
208	0,001	208	0,078	208	0,008
207	0,009	208	0,025	208	0,003
207	0,083	208	0,005	208	0,056
207	0,028	207	0,003	206	0,015
206	0,015	206	0,017	206	0,018
205	0,111	206	0,062	205	0,152
205	0,062	205	0,132	205	0,053
204	0,002	205	0,034	205	0,007
204	0,113	203	0,124	203	0,087
203	0,174	203	0,115	203	0,042
203	0,035	202	0,067	202	0,288
202	0,071	202	0,054	202	0,269
202	0,218	202	0,696	201	0,279
201	0,162	201	0,068	201	0,020
201	0,195	200	0,064	201	0,027
201	0,238	199	0,052	200	0,026
200	0,190	199	0,000	200	0,019

4-(4-(4-Phenoxy)phenoxy)phenoxyphenol (4PPPP)

Six different stable conformational isomers of 4PPPP have been found. In this case as well, the difference among the optimized structures concerns the dihedral angle between the aromatic rings. The name of these angles is the same used in the case of 4PP, adding an apostrophe for the corresponding angles between the second and the third rings and inverted commas for the angles between the third and the fourth ring.
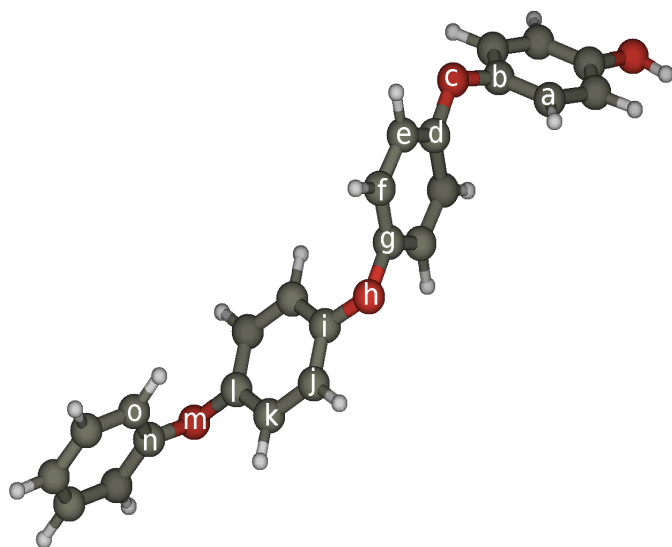
The theta (θ) angle is identified by the atoms a-b-c-d, omega (ω) is identified by atoms b-c-d-e, theta' (θ') is identified by atoms f-g-h-i, omega' (ω') by g-h-i-j, theta" (θ") by k-l-m-n and omega" (ω") by l-m-n-o.

Figure SM5. The 4e conformer of 4PPPP.

Name	(θ)	(ω)	(θ')	(ω')	(θ")	(ω")	Energy ΔG (Kcal/mol)	Weights
4a	109	-9	137	148	58	28	0.242	0.17
4b	93	-1	115	165	129	154	0.201	0.18
4c	-126	-156	130	152	-62	158	0.109	0.19
4d	-70	167	123	158	-121	-161	0.362	0.15
4e	-62	158	-76	-11	67	20	0.000	0.22
4f	-48	-36	-53	-33	55	27	0.878	0.09

Table SM3. *Structure parameters and relative free energies of the 4PPPP conformers.*

Name	(θ)	(ω)	(θ')	(ω')	(θ")	(ω")	ΔEnergy (kcal/mol)	Fluorescence (nm)
4aS1	161	-41	-176	89	64	23	0	448
4bS1	53	35	103	-5	-14	-61	3.038	434
4cS1	-163	-141	4	89	119	-23	0.044	447
4dS1	-22	-46	-2	97	69	18	0.036	446
4eS1	22	41	-4	-87	-62	-24	0.038	446
4fS1	-19	-47	-4	102	73	14	0.017	448

Table SM4. *Structure parameters, relative electronic energies and emission wavelengths of the 4PPPP excited state conformers.*
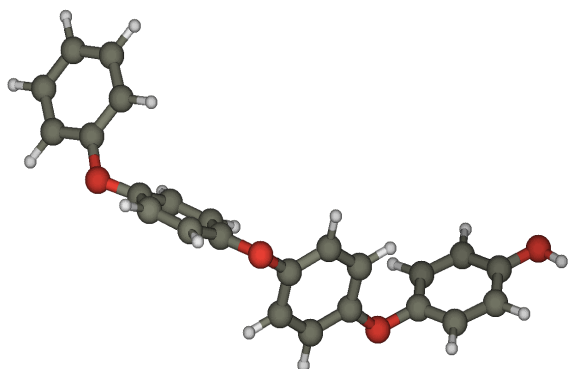
The pictures below show the structures of the ground (4x) and excited states (4xS1) of the conformers of 4PPPP.
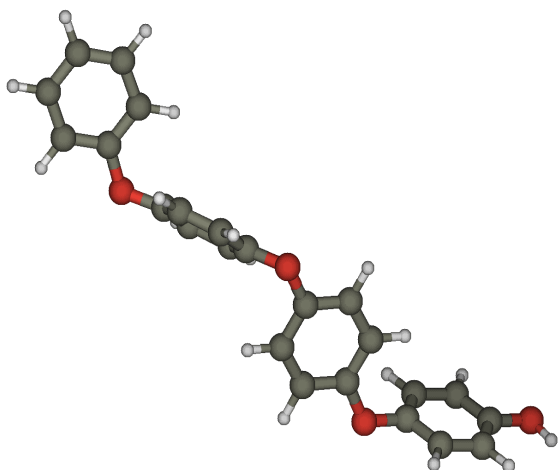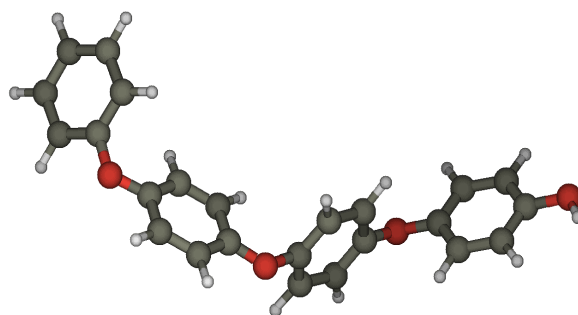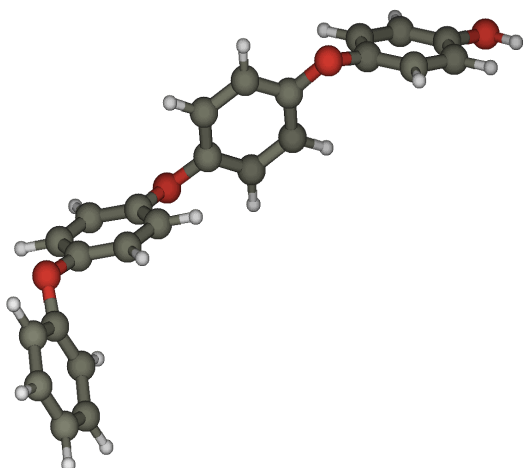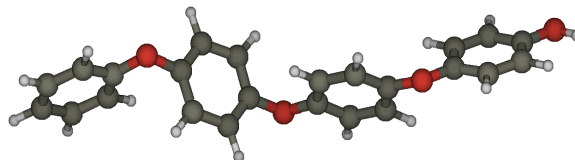

4a

4aS1

4b

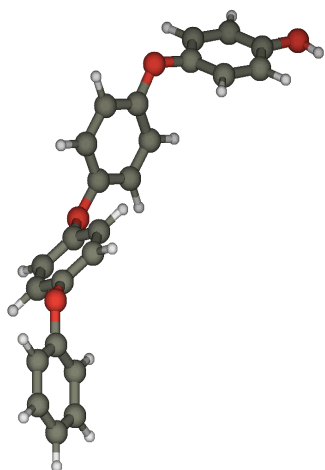

4bS1

4c

4cS1

4d
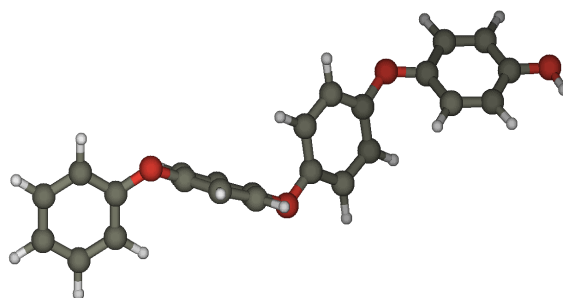
4dS1
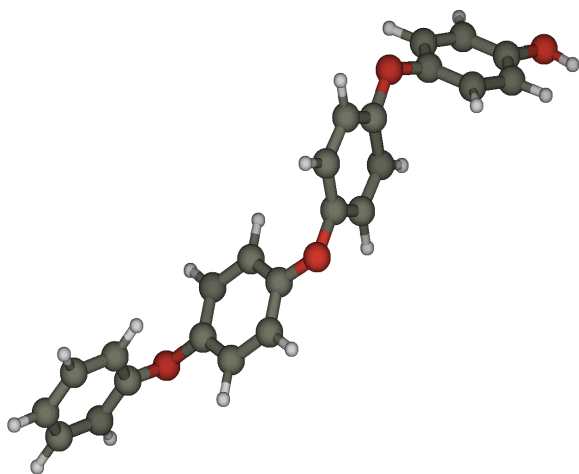
4e
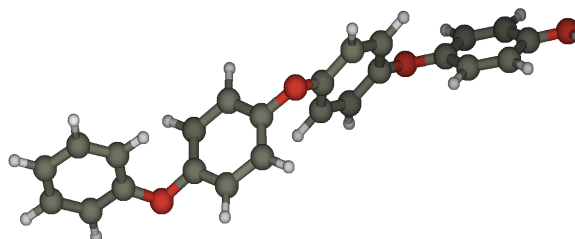
4eS1

4f

4fS1

4a

4b

4c

4d

4e

4f
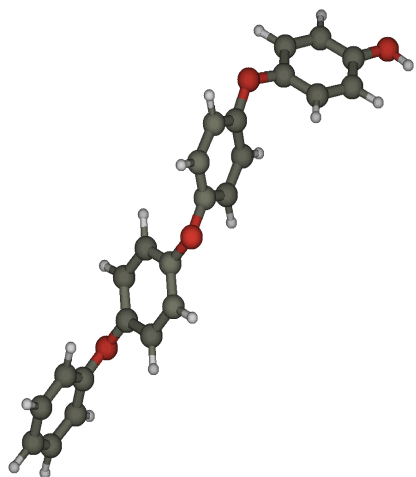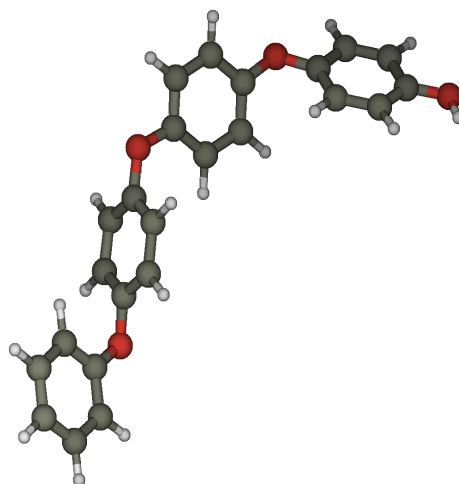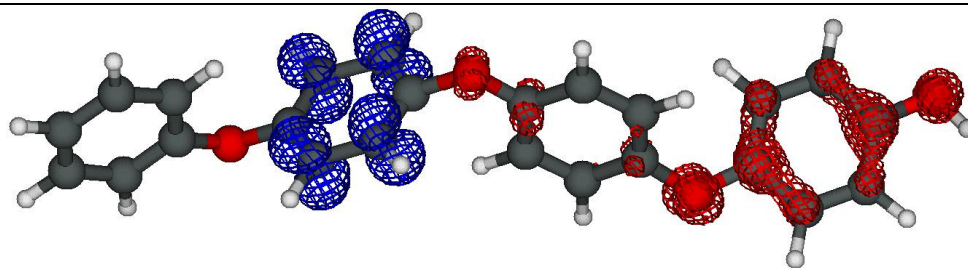
Figure SM6. Differential electronic density map between state S_1 and S_0 in the different conformations of 4PPPP.

The chart below shows the calculated transitions for the different conformers of 4PPPP (wavelengths and the force constants f are reported).

Calculated transitions for 4 rings structures

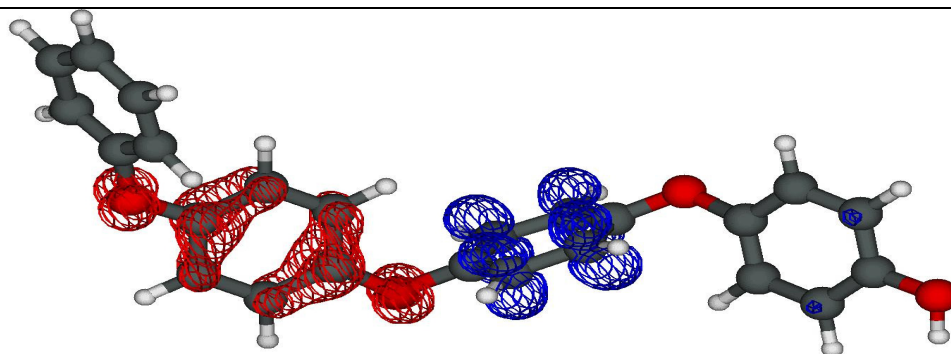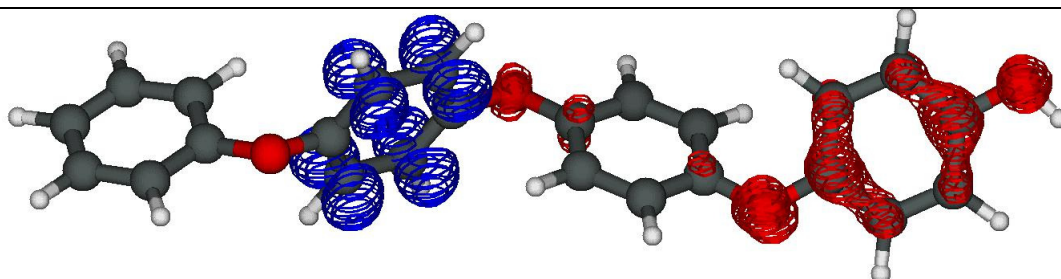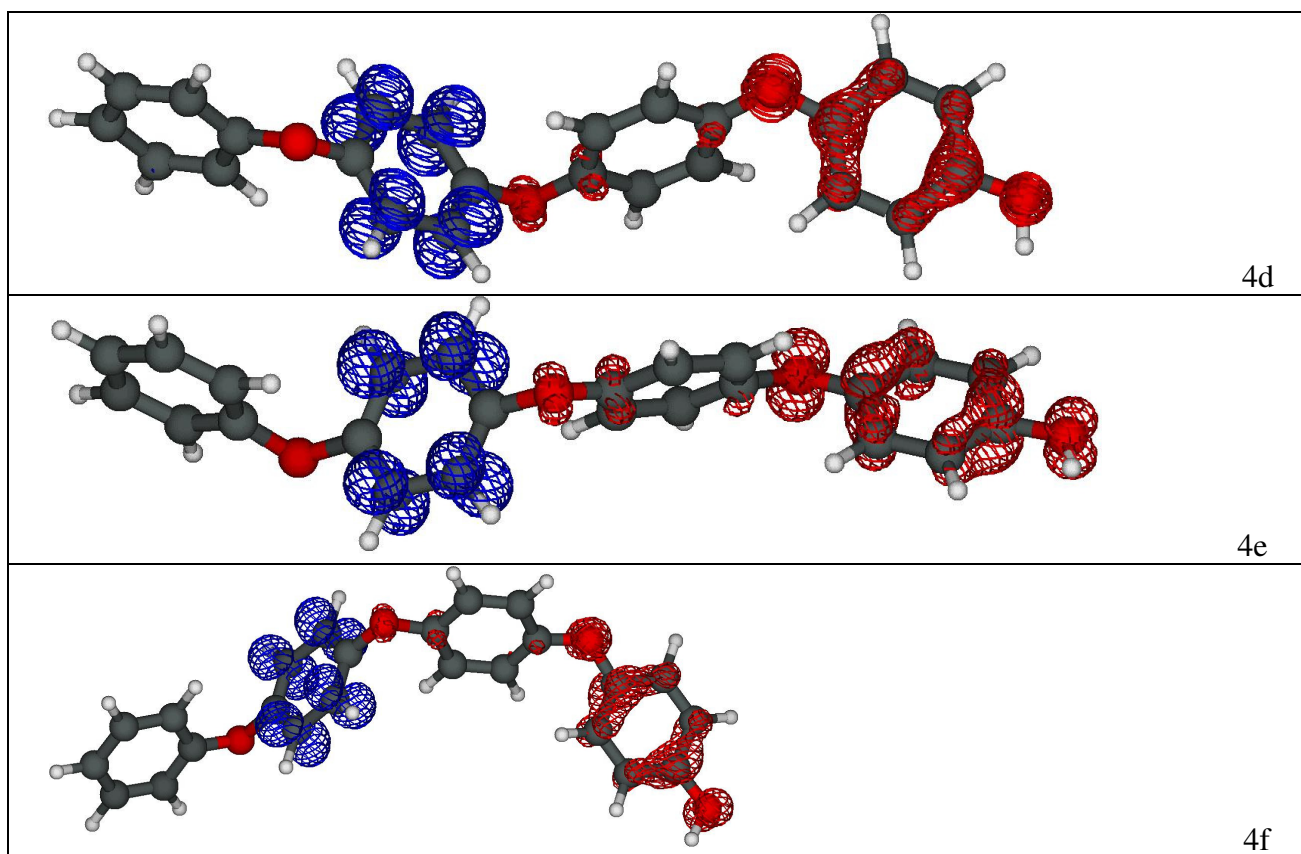| 4a		4b		4c		4d		4e		4f	
λ (nm)	f	λ (nm)	f	λ (nm)	f	λ (nm)	f	λ (nm)	f	λ (nm)	f
349	0,042	342	0,027	352	0,019	345	0,040	342	0,007	357	0,008
339	0,012	327	0,009	338	0,015	335	0,009	335	0,015	342	0,007
323	0,004	320	0,002	327	0,009	323	0,003	322	0,025	332	0,008
320	0,009	317	0,004	321	0,129	316	0,001	314	0,039	327	0,171
318	0,205	309	0,028	319	0,008	312	0,187	309	0,018	321	0,009
311	0,003	304	0,026	311	0,023	308	0,005	307	0,064	316	0,007
306	0,004	303	0,149	309	0,022	306	0,006	304	0,029	311	0,125
304	0,046	301	0,004	306	0,097	302	0,043	302	0,002	310	0,056
301	0,005	298	0,001	301	0,043	301	0,005	301	0,002	304	0,009
299	0,018	297	0,005	300	0,024	298	0,028	298	0,005	301	0,002
297	0,002	296	0,019	298	0,007	294	0,012	294	0,057	298	0,002
294	0,122	291	0,000	290	0,034	290	0,041	291	0,007	292	0,165
287	0,004	288	0,002	288	0,012	289	0,004	288	0,009	290	0,030
286	0,000	284	0,003	286	0,086	285	0,004	286	0,133	290	0,008
284	0,007	282	0,037	285	0,040	283	0,091	285	0,025	286	0,001
283	0,005	282	0,002	284	0,005	281	0,018	281	0,021	285	0,012
279	0,040	279	0,001	283	0,000	280	0,001	276	0,002	283	0,010
277	0,000	278	0,001	277	0,000	276	0,002	276	0,005	279	0,000
275	0,005	276	0,001	275	0,007	276	0,016	275	0,008	274	0,003
275	0,013	274	0,118	274	0,078	274	0,027	273	0,049	273	0,109
274	0,013	272	0,011	273	0,023	273	0,005	271	0,047	272	0,008
271	0,029	271	0,001	270	0,021	270	0,028	270	0,001	270	0,002
269	0,010	269	0,039	268	0,007	270	0,005	269	0,001	269	0,000
267	0,005	268	0,027	267	0,000	268	0,002	268	0,003	268	0,018
266	0,007	267	0,029	267	0,003	266	0,010	267	0,013	267	0,005
266	0,007	266	0,032	266	0,013	265	0,005	267	0,021	266	0,025
263	0,047	264	0,003	266	0,003	264	0,030	266	0,011	265	0,006
263	0,055	262	0,001	262	0,016	264	0,020	264	0,034	264	0,002
262	0,054	260	0,020	261	0,058	262	0,070	262	0,001	261	0,013
260	0,028	259	0,000	261	0,004	260	0,010	260	0,001	260	0,042
257	0,001	258	0,001	260	0,016	259	0,000	259	0,023	258	0,017
256	0,001	258	0,005	256	0,004	258	0,035	257	0,003	257	0,001
255	0,001	257	0,067	255	0,002	257	0,012	256	0,009	255	0,003
255	0,003	256	0,003	255	0,021	255	0,001	255	0,075	255	0,000
254	0,021	253	0,006	254	0,037	254	0,033	254	0,006	253	0,023
253	0,008	253	0,040	252	0,047	253	0,000	254	0,004	253	0,004
252	0,015	253	0,003	252	0,005	252	0,009	252	0,044	252	0,076
252	0,020	252	0,000	252	0,014	252	0,017	252	0,004	252	0,004
250	0,006	252	0,005	250	0,020	251	0,045	251	0,020	251	0,064
250	0,079	251	0,004	250	0,000	250	0,001	250	0,002	249	0,017
249	0,000	251	0,002	249	0,002	250	0,010	248	0,001	248	0,012
248	0,003	247	0,002	247	0,002	248	0,026	246	0,028	247	0,000
248	0,000	245	0,002	246	0,001	247	0,012	246	0,003	247	0,001
247	0,018	245	0,008	246	0,002	246	0,002	246	0,001	246	0,000
246	0,022	244	0,014	245	0,070	245	0,023	245	0,005	246	0,008
245	0,030	244	0,004	245	0,055	245	0,001	243	0,001	245	0,004
244	0,002	243	0,028	245	0,009	244	0,002	243	0,002	245	0,001
243	0,018	243	0,020	244	0,004	243	0,004	243	0,003	244	0,001
243	0,007	242	0,007	243	0,002	242	0,009	242	0,009	243	0,017
243	0,003	241	0,002	242	0,013	241	0,006	240	0,003	242	0,010
241	0,005	240	0,005	242	0,000	241	0,004	240	0,012	242	0,013
241	0,006	239	0,069	241	0,014	240	0,003	240	0,004	242	0,012
240	0,002	238	0,164	241	0,005	239	0,003	239	0,001	241	0,048
240	0,013	238	0,011	239	0,001	238	0,007	238	0,005	241	0,010
239	0,005	238	0,004	238	0,014	238	0,011	238	0,001	240	0,020
239	0,009	238	0,006	238	0,008	238	0,008	237	0,007	238	0,007
238	0,054	237	0,006	237	0,003	237	0,001	237	0,000	238	0,014
237	0,003	236	0,001	237	0,002	237	0,002	236	0,015	238	0,002
236	0,018	236	0,001	237	0,012	237	0,003	236	0,062	237	0,004
235	0,013	236	0,001	236	0,006	236	0,009	235	0,004	236	0,032
235	0,013	236	0,089	236	0,001	235	0,002	235	0,005	236	0,010
234	0,004	234	0,004	234	0,009	234	0,078	235	0,003	236	0,003
233	0,017	234	0,002	233	0,003	233	0,012	235	0,002	235	0,001
233	0,056	233	0,002	233	0,007	233	0,001	234	0,005	235	0,002
232	0,013	232	0,041	233	0,003	232	0,048	233	0,012	234	0,015
232	0,003	232	0,011	232	0,000	232	0,041	232	0,026	233	0,005
231	0,007	231	0,010	232	0,004	232	0,003	232	0,013	233	0,007
231	0,002	231	0,023	231	0,029	231	0,021	231	0,142	231	0,007
230	0,003	230	0,014	231	0,007	230	0,041	231	0,225	231	0,014
230	0,043	230	0,001	230	0,008	229	0,030	231	0,063	231	0,002
230	0,003	230	0,015	229	0,022	229	0,026	230	0,009	230	0,002
229	0,002	229	0,012	229	0,001	229	0,077	229	0,046	229	0,004
228	0,008	229	0,016	228	0,005	229	0,016	229	0,005	227	0,008
228	0,014	228	0,005	228	0,011	228	0,121	229	0,021	227	0,013
228	0,018	227	0,121	227	0,077	228	0,016	228	0,001	226	0,009
227	0,102	227	0,028	227	0,032	227	0,049	228	0,008	226	0,036
226	0,047	226	0,000	227	0,002	227	0,007	227	0,003	226	0,005
226	0,008	226	0,027	226	0,019	226	0,042	226	0,018	225	0,001
226	0,055	226	0,018	225	0,031	226	0,006	226	0,003	225	0,027
225	0,002	225	0,044	225	0,041	225	0,002	225	0,010	225	0,001
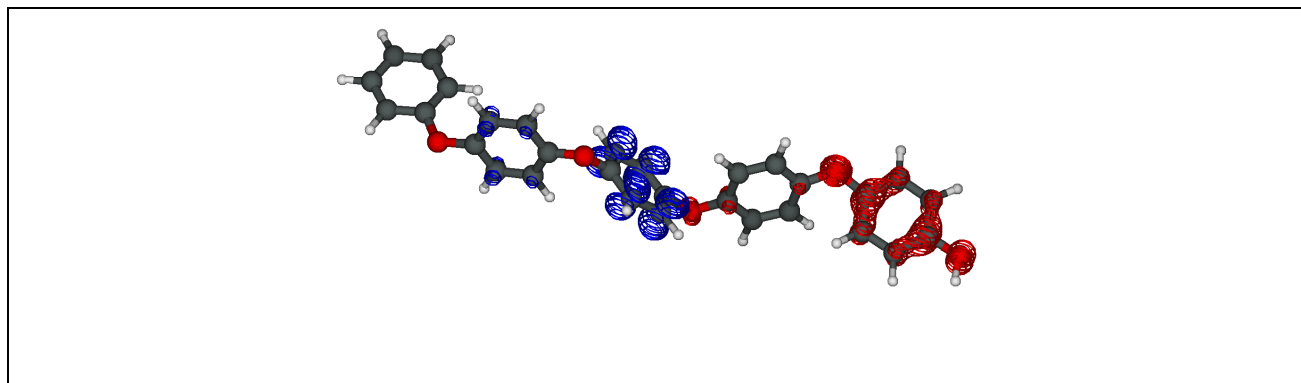
Figure SM7. **Differential electronic density map between state S_1 and S_0 in 4PPPPP.**

3. Weight function and simulated spectra

The calculation of each structure required 80 transitions to be taken into account, starting from the lowest energy one. Such transitions were combined as Gaussian functions with the maximum on the wavelength of each transition. The combination was carried out by using the R language for statistical computing (R Development Core Team, 2008).

As an example, the R script used to combine the absorption spectra of the 2a conformation of PhOPhOH is shown below.

```
a=c(0.0270,0.0068,0.0085,0.0007,0.0328,0.0232,0.0005,0.0079,0.0007,0.0051,0.010
0,0.0006,0.3019,0.0164,0.0318,0.0171,0.0033,0.0042,0.0199,0.0039,0.0729,0.0001,
0.0015,0.0042,0.0014,0.0005,0.0019,0.0237,0.0165,0.0001,0.1806,0.0307,0.1687,0.
0421,0.1413,0.0833,0.6587,0.0310,0.0256,0.0335,0.0071,0.0487,0.1438,0.0543,0.10
29,0.0065,0.0258,0.0118,0.0059,0.0023,0.0012,0.0025,0.0097,0.0001,0.0000,0.0021
,0.0203,0.0029,0.0027,0.0012,0.0076,0.0398,0.0030,0.0059,0.0073,0.0104,0.0324,0
.0173,0.0033,0.0023,0.0665,0.0266,0.0324,0.0017,0.0077,0.0024,0.0168,0.0144,0.0
057,0.0074)

b=c(301,297,275,273,267,263,257,254,252,247,242,242,236,235,233,232,228,227,225
,222,221,221,219,214,214,213,210,208,207,206,205,205,203,202,202,201,200,197,19
7,196,196,195,194,193,192,191,191,188,188,187,186,185,184,184,183,183,182,181,1
80,180,179,178,177,177,177,176,176,175,174,173,173,173,172,172,171,171,170,170,
169,169)

c=c(3.5)

xmin<c(200)
```

```
xmax<c(360)

x<seq(xmin,xmax,length.out=200)

nx=length(x)

ng=length(b)

y=data.frame(NULL)

for (i in 1:ng) {

    for (j in 1:nx) {

    y[i,j]=(a[i]*exp(((x[j]b[i])^2)/(c^2)))          }}

colsum<colSums(y)

tabella<data.frame(x,colsum)

write.csv(tabella,file="PhOPhOH_acqua.csv")
```
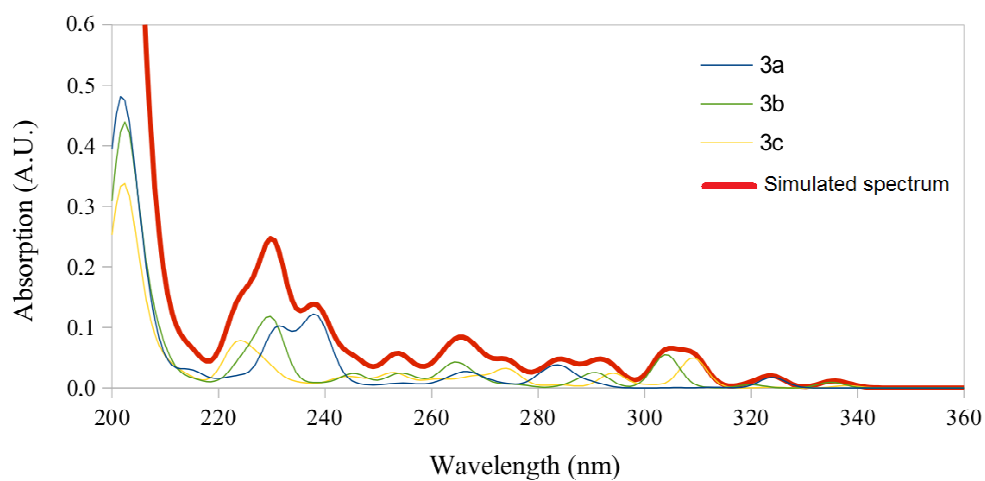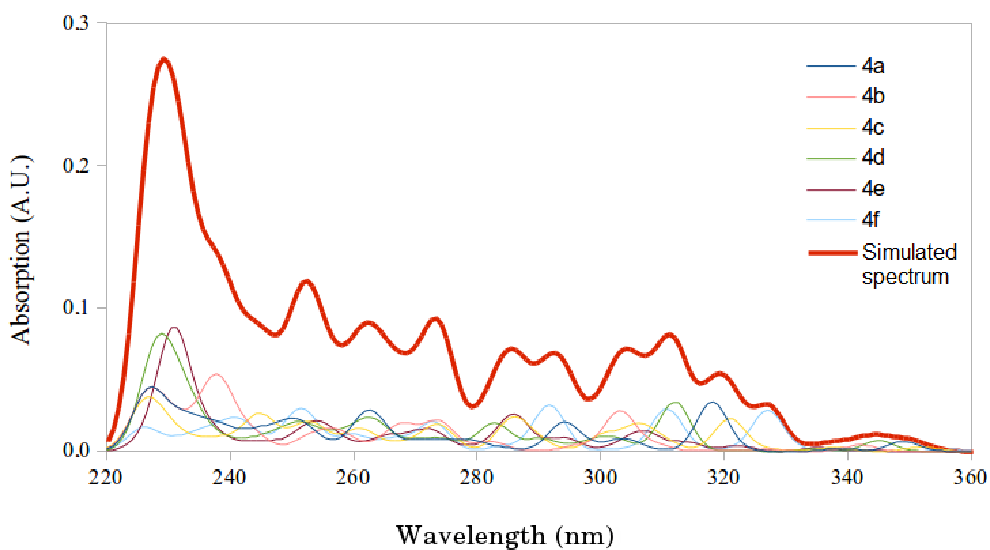
The spectra of the different conformations were then linearly combined, by weighting for the different energy of the structures. The weight of each conformation was calculated as shown in the equation below:

$$w_i = \frac{e^{-\frac{E_i}{RT}}}{\sum e^{-\frac{E_i}{RT}}}$$

where E_i is the energy of the ith conformation and N is the number of considered conformations, three in this case (2a, 2b and 2c). In this way one obtains the simulated absorption spectra, which give some insight into the possible absorption of radiation by compounds for which standards are not available. The figures below show the simulated absorption spectra of 4PPP and 4PPPP.

Figure SM8. Spectra of the different conformations of 4PPP and their linear combination (simulated spectrum).

Figure SM9. Spectra of the different conformations of 4PPPP and their linear combination (simulated spectrum).

4. References

Adamo, C., Barone, V., 1998. Exchange functionals with improved long-range behavior and adiabatic connection methods without adjustable parameters: The mPW and mPW1PW models. J. Chem. Phys. 108, 664-675.

Becke, A. D., 1988. Density-functional exchange-energy approximation with correct asymptotic-behavior Phys. Rev. A 38, 3098-3100.

Becke, A. D., 1993. Density-functional thermochemistry. III. The role of exact exchange. J. Chem. Phys. 98, 5648-5652.

Burke, K., Perdew, J. P., Wang, Y., 1998. Electronic Density Functional Theory: Recent Progress and New Directions. Dobson, J. F., Vignale, G., Das, M. P. (eds.), Plenum Press.

Davidson, E. R., 1996. Comment on "Comment on Dunning's correlation-consistent basis sets". Chem. Phys. Lett. 260, 514-518.

Dunning T. H. Jr., 1989. Gaussian basis sets for use in correlated molecular calculations. I. The atoms boron through neon and hydrogen. J. Chem. Phys. 90, 1007-1023.

Ernzerhof, M., Perdew, J. P., 1998. Generalized gradient approximation to the angle- and system-averaged exchange hole. J. Chem. Phys. 109, 3313-3320.

Henderson, T. M., Izmaylov, A. F., Scalmani, G., Scuseria, G. E., 2009. Can short-range hybrids describe long-range-dependent properties? J. Chem. Phys. 131, 044108.

Heyd, J., Scuseria, G., Ernzerhof, M., 2003. Hybrid functionals based on a screened Coulomb potential. J. Chem. Phys. 118, 8207-8215.

Izmaylov, A. F., Scuseria, G., Frisch, M. J., 2006. Efficient evaluation of short-range Hartree-Fock exchange in large molecules and periodic systems. J. Chem. Phys. 125, 104103.

Kendall, R. A., Dunning,T. H. Jr., Harrison, R. J., 1992. Electron affinities of the first-row atoms revisited. Systematic basis sets and wave functions. J. Chem. Phys. 96, 6796-6806.

Lee, C., Yang, W., Parr, R. G., 1988. Development of the Colle-Salvetti correlation-energy formula into a functional of the electron density. Phys. Rev. B 37, 785-789.

McLean, A. D., Chandler, G. S., 1980. Contracted Gaussian-basis sets for molecular calculations. 1. 2nd row atoms, Z = 11-18, J. Chem. Phys. 72, 5639-5648.

Perdew, J. P., Burke, K., Ernzerhof, M., 1996. Generalized gradient approximation made simple. Phys. Rev. Lett. 77, 3865-3868.

Perdew, J. P., Burke, K., Wang, Y., 1996. Generalized gradient approximation for the exchange-correlation hole of a many-electron system. Phys. Rev. B 54, 16533-16539.

Perdew, J. P., Burke, K., Ernzerhof, M., 1997. Errata: Generalized gradient approximation made simple. Phys. Rev. Lett. 78, 1396.

Petersson, G. A., Bennett, A., Tensfeldt, T. G., Al-Laham, M. A., Shirley, W. A., Mantzaris, J., 1988. A complete basis set model chemistry. I. The total energies of closed-shell atoms and hydrides of the first-row atoms. J. Chem. Phys. 89, 2193-2218.

Petersson, G. A., Al-Laham, M. A., 1991. A complete basis set model chemistry. II. Open-shell systems and the total energies of the first-row atoms. J. Chem. Phys. 94, 6081-6090.

Raghavachari, K., Binkley, J. S., Seeger, R., Pople, J. A., 1980. Self-consistent molecular orbital methods. 20. Basis set for correlated wave-functions, J. Chem. Phys. 72, 650-654.

Tao, J. M., Perdew, J. P., Staroverov, V. N., Scuseria, G. E., 2003. Climbing the density functional ladder: Nonempirical meta-generalized gradient approximation designed for molecules and solids. Phys. Rev. Lett. 91, 146401.

Yanai, T., Tew, D., Handy, N., 2004. A new hybrid exchange-correlation functional using the Coulomb-attenuating method (CAM-B3LYP). Chem. Phys. Lett. 393, 51-57.

Zhao, Y., Truhlar, D. G., 2006. The M06 suite of density functionals for main group thermochemistry, thermochemical kinetics, noncovalent interactions, excited states, and transition elements: two new functionals and systematic testing of four M06-class functionals and 12 other functionals. Theor. Chem. Acc. 120, 215-241.